GRID PLANNING ALGORITHM UNDER UNCERTAINTIES FOR AN OPTIMAL INTEGRATION OF ELECTRIC VEHICLES

Lappeenranta–Lahti University of Technology LUT

Energy Technology Master of Science, Triple Degree 2021

Tammo Wegener

Examiner: Prof. Jamshid Aghaei

Prof. Dr.-Ing. habil. L. Hofmann

Declaration:

I declare that this thesis has been composed solely by myself and that it has not been submitted, in whole or in part, in any previous application for a degree. Except where stated otherwise by reference or acknowledgment, the work presented is entirely my own.

Hannover, the 13.10.2021 Tammo Wegener

Abstract

With the integration of electric vehicles charging infrastructure into the medium and low voltage grid, new challenges for the distribution grid operators arise. The power demand due to electric vehicle charging occurs with high simultaneity and power compared to the conventionally connected dwelling loads. In order to effectively integrate electric vehicles into the existing grids, methods are required to prevent voltage band violations and the over-utilization of lines, which could threaten smooth grid operation.

A classic approach to overcome grid bottlenecks, based on the NOVA principle, is the reinforcement of grids. This work investigated the cost effective reinforcement of low voltage networks that have been overloaded due to the integration of electric vehicle charging equipment, using a grid reinforcement algorithm. For this investigation, the cigre benchmark network was utilized based on which, basic assumptions were made regarding the number and charging power of electric vehicles. The number of dwellings within the benchmark grid was derived using the simultaneity factor for different degrees of household electrification, while the quantity of electric vehicles was estimated using current vehicle statistics and future set goals by the government. Furthermore, the costs for different grid reinforcement options in urban areas was established. Novel methods using conventional grid reinforcement, variable transformers, lithium-ion storage and combined heat and power were considered. Using the load torque approach and sensitivity matrices, the most vulnerable grid nodes were ascertained. In addition, uncertainties due to cable temperature and temperature coefficient were depicted and evaluated using a Monte-Carlo simulation.

In this thesis, it has been found that the grid reinforcement costs for the integration of electric vehicle charging equipment across the grid can be accurately estimated by placing all charging equipment at a single grid node. To determine the maximum and minimum grid expansions costs, it is sufficient to analyse the most and least sensitive grid nodes. This leads to a reduction of required computational power, since only two grid nodes need to be taken into consideration. Additionally, the cost influences of cable uncertainties are less than 4 %, and variable transformer are not a viable option to circumvent conventional grid reinforcement when considering the integration of larger amounts of electric vehicle charging equipment. Furthermore, grid reinforcement using lithium-ion storage is 10,6 times more expensive in comparison to conventional grid reinforcement, even when taken predicted lithium-ion battery prices for 2025. As for combined heat and power reinforcement costs, the applicability without making use of the extant heat is compared to the conventional grid reinforcement costs is 5,7 times greater is comparison to the cost for conventional grid reinforcement.

Kurzzusammenfassung

Mit dem Zuwachs von Ladeinfrastruktur für Elektrokraftfahrzeugen (E-Kfz) treten für den Netzbetreiber im Mittle- und Niederspannungsnetz neue Herausforderung auf. Das Laden von E-Kfz erfolgt im Vergleich zu gewöhnlichen Haushaltslasten mit hoher Gleichzeitigkeit und Ladeleistung. Um Spannungsbandverletzungen und die Überlastung von Leitungen zu verhindern sind Methoden zum Überwinden solcher Netzengpässe gefragt.

Ein klassisches Modell zum Überwinden von Netzengpässen ist das NOVA Prinzip. In dieser Arbeit werden die Kosten zur effektiven Verstärkung von Niederspannungsnetzen, welche durch den Zuwachs von Ladeinfrastruktur hervorgerufen werden, mithilfe eines Netzverstärkungsalgorithmus erforscht. Die Verstärkung des Netzes wurde anhand des cigre Benchmark Netzwerkes untersucht. Unter Zuhilfenahme des Gleicheichzeitigkeitsfaktors für unterschiedliche elektrische Durchdringungen von Hauhalten, wurde die Anzahl an Haushalten im Testnetz ermittelt. Basierend auf aktuellen Fahrzeugstatistiken und zukünftigen Zielen der Bundesregierung wurde die durchdringung von E-Kfz Ladeinfrastruktur identifiziert. Darüber hinaus wurden die unterschiedlichen Kosten zur Netzverstärkung aufgestellt. Die ausgewählten Methoden zur Netzverstäkung sind: Konventionelle Netzverstärkung, regelbare Ortsnetztransformator, Lithium-Ionen Speicher und Blockheizkraftwerke. Unter Berücksichtigung des Drehmomentansatzes und der Sensitivitätsmatrizen wurden die anfälligsten Netzknoten identifiziert. Desweiteren wurden als Unsicherheitsfaktoren die Leitertemperatur und der Leitertempkoeff mithilfe einer Monte-Carlo Simulation abgeschätzt.

Die Ergebnisse dieser Arbeit zeigen, dass es möglich ist entstehende Netzverstäkungskosten durch die Integration von Ladeinfrastruktur anhand einer konzentrierten Platzierung dieser an einen einzigen Netzknoten abzuschätzen. Zur Identifizierung der maximalen und minimalen Netzverstärkungskosten ist eine Analyse der am stärksten und schwächsten sensitiven Knotenpunkte ausreichend. Hierdurch ist es möglich, die benötigte Rechenleistung zu Reduzierung. Die Auswirkungen von Unsicherheitsfaktoren auf die Netzverstärkungskosten betragen bis zu 4 %. Zugleich ist der Einsatz regelbarer Ortsnetztransformatoren zum Umgehen der konventionellen Netzverstärkungskosten nicht wirtschaftlich. Beim Vergleich der unterschiedlichen Kosten für die Netzverstärkungmethoden konnte festgestellt werden, dass die Netzverstärkungskosten für Lithium-Ionen Speicher, unter Annahme von projezierten Preisen für 2025, um den Faktor 10,6 kostspieliger sind als konventionelle Netzverstäkung. Blockheizkraftwerke sind unter Vernachlässigung der Wärmeauskopplung um den Faktor 5,7 teurer als konventionelle Netzverstärkung.

Contents

List of Figures

List of Tables

Acronyms

CHP	Combined heat and power
DER	Distributed Energy Resource
EVCQ	electric vehicle charging equipment
EVCU	electric vehicle charging unit
HV	High voltage
IfES	Institut of Electronic Power Systems
IQR	Interquartile range
LUH	Leibniz University Hannover
LV	Low voltage
MV	Medium voltage
PV	Photovoltaic
VDE	Association for Electrical, Electronic & Information Technologies

List of Symbols

A	Annuity factor
α_0	Temperature coefficient
$\mathbf{B}$	Inverse Jacobian
C'	Insulator capacitance
δ	Phase angle
g	Simultaneity factor
g_∞	Convergence factor
γ	Propagation constant
G'	Insulator conductance
I	current
I_{idle}	Idle transformer current
$\underline{i}_{\text{K}}$	Node current vector
I_{i}	magnetizing current
I_{r}	Load capacity
Z	Impedance
i_{T}	Terminal current
I_{th}	Current carrying capacity
$\mathbf{J}$	Jacobian matrix
k_0	Acquisition cost
k_{A}	Associated equipment cost
k_{cable}	Cable cost
k_{cap}	Storage unit capacity cost
k_{CHP}	CHP cost
k_{coup}	Coupling cost
k_{E}	Equipment/Machinery cost
k_{L}	Labor cost
k_{oper}	Operational Cost
k_{Sto}	Total storage unit cost
k_{T}	Transmission network cost
k_{total}	Total grid expansion cost
l	Line length
L'	Loop inductance
μ	Mean
n_{WE}	Number of households
ν	Iteration step
P	Active power
P_{max}	Maximum power draw

P_{maxLA}	Peak power share
P_{S}	Peak power draw
Q	Reactive power
R	Resistance
R_0	Reference resistance
R_{Fe}	Iron core resistance
R'	Loop resistance
S	Apparent power
S_{rT}	Rated transformer power
$\underline{s}_{\mathrm{T}}$	Terminal power vector
σ	Standard deviation
t_{use}	Lifetime
U	Voltage
$\underline{\mathbf{U}}_{\mathrm{K}}$	Node voltage matrix
$\underline{u}_{\mathrm{K}}$	Node voltage vector
u_{k}	Short circuit voltage
U_{rTOS}	Rated transformer voltage high voltage side
U_{rTUS}	Rated transformer voltage low voltage side
u_{T}	Terminal voltage
ü	transformation ratio
φ	Phase shift/power factor
ϑ_0	Reference temperature
ϑ_C	Current temperature
X	Complex resistance
X_{h}	Main inductance
X_σ	Leakage inductance
Y	Admittance
$\underline{\mathbf{Y}}_{\mathrm{KK}}$	Nodal admittance matrix
$\underline{\mathbf{Y}}_{\mathrm{KT}}$	Nodal terminal incidence matrix
$\underline{\mathbf{Y}}_{\mathrm{T}}$	Terminal admittance matrix
$\underline{\mathbf{Y}}_{\mathrm{Tl}}$	Line admittance matrix
$\underline{\mathbf{Y}}_{\mathrm{Tt}}$	Transformer admittance matrix

1 Introduction

The rapidly developing climate change is affecting people all around the globe. To cope with the defining crisis of our time the Paris Agreement was established in 2016. The 196 countries that signed the agreement pledge to reduce greenhouse gas emissions in an effort to become climate-neutral. [48]. The European Union reaffirmed its commitment towards this goal by increasing the targeted emission reduction goal by 15 %. Thereby all members of the European Union need to cut greenhouse gas emissions by at least 55 % by 2030 [44]. Germany, being a member of the European Union and emitting the highest amount of carbon dioxide within it [69], will therefore have the most impact on the overall reduction of greenhouse gases.
The three sectors most responsible for CO_2 emissions in Germany are energy, industry and transportation [70]. Even through the energy and industry sector were able to greatly reduce their emissions since 1990, the transportation sector stayed almost constant. In an effort to reduce carbon emissions produced by vehicles, the German electrical mobility program was enacted [50]. This kicked off a fundamental transformation in the automotive industry. The cornerstone to a transition from gasoline to electrically driven cars was set by the program. To demonstrate the governments commitment in this sector the program was revised as of 2020 in an effort to fast track the adoption of electric vehicles.

1.1 Motivation

Traditionally, vehicles are refueled at gas stations, which obtain their fuel using trucks or pipelines. With the rise of electric vehicles the burden of refuelling gets shifted to the electricity network. Electric vehicles are recharged using electric vehicle charging equipment (EVCQ), that can virtually be installed anywhere along the distribution grid. The exponential growth in electric vehicles registrations [61] therefore leads to a substantial load increase within the distribution grid. In order to have a secure and reliable energy supply, according to §1 of the energy economy law [51] in the future, network operators are facing new challenges regarding grid bottlenecks and voltage stability. Existing grid structures have been planned on the assumption of conventional load requirements. The increasing amount of unknown fluctuating load demands thorugh electric vehicles [21] leads to new types of stress on the distribution grid. This poses new challenges in the field of power system stability, due to overloaded transformers or lines.
To successfully cope with future electricity demand caused by EVCQ, an investigation into the future should be performed; ascertaining optimal and cost effective grid development methods, which can lead to an effective and environmental electric vehicle transition.

1.2 Aim of this Thesis

The aim of this thesis is the cost effective improvement of low voltage of girds, which are not able to satisfy the additional load flow demand occurring through the integration of electric vehicle charging equipment. To achieve this, proper grid improvement variants need to be determined, which should be investigated with the help a suitable network and algorithm. Within the scope of this investigation, a scenario analysis to derive different electric vehicle penetration levels should be ascertained. Furthermore, the usability of innovative equipment, such as energy storage units and variable transformers should be explored. Potential uncertainties by variable grid parameters should additionally be considered.

2 Fundamentals

This chapter aims to briefly explain the basic terms and mathematical methods that have been applied during this work. To solidify the main approach chosen for this work, the NOVA principle is outlined in the beginning. Upon the selected approach, alternative methods to circumvent conventional grid development are outlined. Following this, is the simultaneity factor. Next the electrical modelling of utilities and classic grid topologies are discussed. This is done to set the framework for power flow calculations, which will be used throughout. In order to assess those calculations, the main grid operational limits are identified. This is followed by grid restrictions, which transition into methods for determining the most detrimental grid points within a network. To account for uncertainties in lines, the Monte-Carlo simulation is present at the end of the chapter.

2.1 NOVA Principle

The goal of every network operator is to avoid grid bottlenecks. Bottlenecks occur whenever the existing grid is unable to satisfy load flow demands. To overcome this the grid needs to be improved. In order to save space and affect nature and humans as little as possible the German NOVA-principle is applied. Directly translated the NOVA-principle stands for network optimization, before network reinforcement, before network expansion. This principle is applied throughout all voltage levels in Germany when developing electricity networks. A brief explanation of every letter and it's meaning according to the German ministry of economy and energy [40] is in the following.

O - Optimization

When bottlenecks are occurring within the network, the load flow must firstly be optimized. This can be done by installing monitoring equipment at the lines to operate them dependent on the weather. For Example, if the ambient temperature drops, a line can carry more energy, since the heat losses resulting from higher power flows can be dissipated better. The exact amount of energy that can be transported depends on the lines individual temperature and its temperate and current ratings.

V - Reinforcement

If line optimization is not possible anymore, the grid needs to be reinforced. This is done by placing more cables or upgrading existing cables. The increase in current carrying capacity allows for additional power to transported.

A - Expansion

Only when grid bottlenecks can be circumvented neither by optimization nor reinforcement the grid will be expanded. This is done by finding new line paths, thereby linking two gird point with each other, that previously haven't been connected.

The focus of this work is limited to grid reinforcement. The other two possibilities (optimization & expansion) are not considered.

2.2 Distributed Power Generation

To avoid sometimes impossible or extremely costly reinforcement of the grid, alternative power generation methods are available. These Distributed Energy Resources (DERs) can be divided into two groups, constant power and infrequent power. Constant power generation methods are able to produce at any given time a minimum amount of power, while infrequent ones are dependent on the current conditions and cannot produce a constant amount of power througout the whole year. The following list displays the currently most common technologies that are in use for decentralized power generation.

- Constant Power
  - CHP
  - Microgasturbine
  - Hydro Power
- Infrequent Power
  - Solar Power
  - Wind Power
  - Energy storage systems

CHP, Microgasturbines and energy storage systems can be rather small (5 kW, < 1 m^2) [43][38], while the other technologies have bigger footprints and environmental impacts. Depending on the geographical location, the construction of bigger power plants can become challenging in LV grids. More than 75 % of the German population lives in cities/urban areas, where space is limited [71]. Therefore only three technologies can be used for local distributed power generation in those areas (CHP, Microgasturbine & Energy storage). During this work only the CHP and energy storage systems are investigated.

2.2.1 Energy Storage

Energy storage systems are not able to supply a constant amount of power indefinitely. The storage system must be recharged after it's depleted. Therefore, a grace period is needed, were the extra power of the energy storage system is not required. Electric vehicles need constant power for charging, but only for the duration of the charging process. The charging process is limited to a defined amount of time for every vehicle. Using home chargers with charging powers of up to 3 kW, the time it takes to charge an electric vehicle to drive 160 km is on average a little greater than 10 hours [25]. According to this, modern electric cars would need more than 24 hours to fully recharge. Fortunately, the mean annual driving distance is 25105 km annually [24]. Therefore every electric vehicle only travels approximately 80 km per day, if only business days are considered. This results in a charging time of approximately 8 hours every day. Due to this, the energy storage unit only needs to be able to supply a constant amount of power for 8 hours and can recharge the remaining day, thereby staying a viable alternative.

The most common types of electrochemical battery systems on the market are lead-acid and lithium-ion. Although lead-acid batteries are by far the most common type of electrochemcial battery on the market in the scope of grid energy storage systems, the trend is slowly shifting towards lithium-ion batteries. Lead-acid batteries are already well researched, and no more major power gains are to be expected. This means, there are no more large reductions in price per kWh to be expected. In contrast to lead-acid are lithium-iron batteries, which have greater energy density & power density and still have future research potential. For this reason the energy storage price for lithium-iron batteries are predicted to be on part with lead-acid batteries by 2025. [14]

2.2.2 Combined Heat and Power

More than 60 % of all electrical power generated in 2017 by CHPs was done using natural gas as fuel [58]. The change from natural gas to green gas produced by biogas and hydrogen plants is already happening [47], in order stay in line with the government goal to producing less carbon emissions [44]. Therefore CHP are staying a vital and reliable option in future.

Operating CHPs to compensate power peaks is not cost effective. Typically smaller CHPs need to operate at least 6000 $^{h}/_{a}$ and their excess heat needs to be used in order to make them economically beneficial [43]. In residential areas the accruing heat can be fed into district heating grids if available. Because of the economical aspects, CHPs should mainly be used to cover the base load. This means, that the plant should operate constantly and the existing grid should be used to cover the occurring peak loads. During this work the CHP will be scaled to the additional power required through EVCQ, but never be increased

past the base load of the network. More precisely the CHP will be sized according to the base load attached to the node at which it is installed. Therefore, the plant is operating at least 6000 h throughout the year.

2.3 Simultaneity Factor

Generally the simultaneity factor is used to estimate the electrical load for residential areas, houses and electrical facilities, for the purpose of network planning. This is done, because the connection power only reflects the sum of all installed power in extreme cases. Normally, not all loads inside a grid draw their power at the same time. Therefore, the assumed electrical loads equal the yearly maximum loads that can be expected. In order to emulate various housing configurations, different levels of electrification (EG) have been devised (see table 8.4). Each level of electrification has a different peak power draw $P_{\mathrm{S,i}}$ and convergency factor g_∞, that represent the quotient from peak power share $P_{\mathrm{maxLA,i}}$ and maximum power draw P_{max}. [3]

Using the simultaneity factor g_i and the yearly maximum power draw $P_{\mathrm{max},i}$ of every single consumer/household n, it is possible to calculate the peak power share [3]:

$$P_{\mathrm{maxLA},i}\left(n_i\right) = g_i\left(n_i\right) \cdot P_{\mathrm{max},i} \tag{2.1}$$

The maximum power draw is made up from the number of loads/households connected to the grid and the average yearly power consumption $P_{\mathrm{S},i}$ of each individual consumer [3]:

$$P_{\mathrm{max},i} = n_i \cdot P_{\mathrm{S},i} \tag{2.2}$$

By applying different levels of electrification, it is possible to estimate various yearly peak loads for any number of households n_{WE} [6]:

$$g\left(n_{\mathrm{WE}}\right) = g_\infty + \left(1 - g_\infty\right) \cdot n_{\mathrm{WE}}^{-3/4} \tag{2.3}$$

During this work, the simultaneity factor is used in the opposite way. By rephrasing the above mentioned equations into the following, the number of households n_{WE} can be determined, based on the average maximum peak power share. Solving the following equation for its roots will result in the number of households.

$$P_{\mathrm{maxLA}} \cdot \varphi = \left(g_\infty + (1 - g_\infty)\, n_{\mathrm{WE}}^{-3/4}\right) P_{\mathrm{S,WE}} \cdot n_{\mathrm{WE}} \tag{2.4}$$

2.4 Equipment Modelling

Utilities can either be described as twopoles or quadropoles. Twopoles, like the name suggests, have only two terminals and can only connect to one node. Generally, consumer loads and power injections are modeled using this variant. Transformers and lines are modeled as quadrupols and can be represented by the general equivalent circuit shown in Figure 2.1. Using the admittance matrix $\underline{\boldsymbol{Y}}_{\mathrm{T}}$, the two terminals A and B, can be set in relation to each other (see equation 2.5).

Figure 2.1 Exemplary schematics depiction of a quadrupol

The currents at each terminal can be described using the following equation [19]:

$$\underline{\boldsymbol{i}}_{\mathrm{T}} = \underline{\boldsymbol{Y}}_{\mathrm{T}}\ \underline{\boldsymbol{u}}_{\mathrm{T}} \tag{2.5}$$

Based on the equipment, the admittance matrix changes. Depending on the number of terminal pairs, each equipment can be categorized into one of the four types A, AB, ABC, ABCD. Generators, motors, equivalent networks, non-linear loads, capacitorbanks and choke coils are described by type A equations. During power flow calculations, type A equipment is represented via voltage dependent sources without any parallel admittances. Type AB equipment represents lines and two-winding transformers, with special consideration for non symmetrical admittances of the transformer. Three-winding transformers are of type ABC, due to the symmetrical component equivalent circuit having six poles, which can be combined into one matrix. The last type ABCD are equations for double/multiple lines. Due to the cables strands being intertwined all symmetrical components are linked with each other. [9]

Generally, symmetrical loads and power injections are assumed for energy networks. This means that in fault free operation, the symmetrical components systems are fully decoupled

and only the zero system equivalent circuit has to be taken into account. Therefore the respective quadrupol equations for a two-winding transformer and line will be derived in the following.

Two-winding Transformer

Two-winding transformers can be represented using the T-equivalent circuit shown in figure 2.2. Terminal A is generally assumed to be the high voltage terminal, while B is the low voltage terminal [19]. The apostrophe on the B elements denotes that the elements are referenced to the high voltage terminal. This is done by applying the transformation-ratio $\underline{\ddot{u}}$ to the low voltage elements.

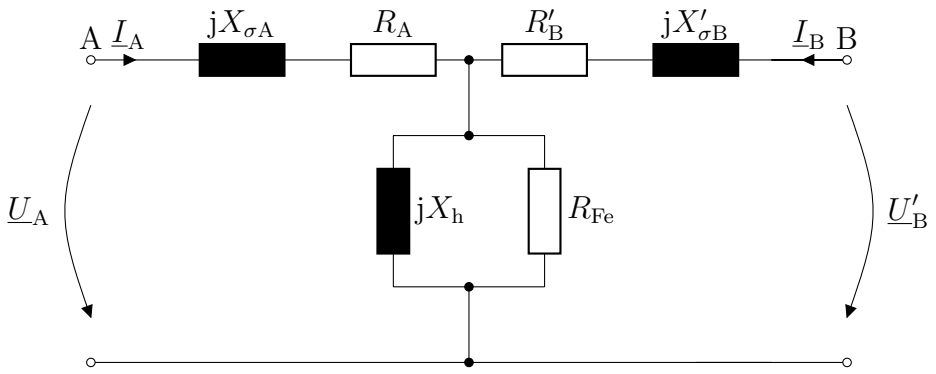

Figure 2.2 T-equivalent circuit of a transformer

In contrast to an ideal transformer losses, have to be considered in a real transformer. The elements in figure 2.2 can be determined using the open-circuit and short-circuit test. During the short-circuit test the iron core losses are neglected in order to determine the horizontal parameters (A and B). Using the rated voltage U_rT, the rated power S_rT as well as the short circuit voltage u_k, the short circuit impedance Z_AB can be determined [4]:

$$Z_\mathrm{AB} = u_\mathrm{k} \cdot \frac{U_\mathrm{rt}^2}{S_\mathrm{rt}} \tag{2.6}$$

Using rated current I_rt and the losses P_Vkr, that have been determined during the short circuit test, the horizontal resistance R_AB, as well as the reactance X_AB can be calculated using the following two equations. [4]

$$R_\mathrm{AB} = \frac{P_\mathrm{Vkr}}{3 \cdot I_\mathrm{rt}^2} \tag{2.7}$$

$$X_{\mathrm{AB}} = \sqrt{Z_{\mathrm{AB}}^2 - R_{\mathrm{AB}}^2} \tag{2.8}$$

Generally, the resistance and reactance will be divided equally to the high and low voltage side Elements [4]. This means that $X_{\sigma\mathrm{A}}$ and $X'_{\sigma\mathrm{B}}$ are both half the amount of X_{AB}.
The iron losses can be determined by applying the open-circuit test. The horizontal elements can be neglected due to their dwindling size compared to the main field impedance. The measured eddy current and hysteresis losses inside the iron core P_{VLr} will be represented using an iron loss resistance R_{Fe}. [4]

$$R_{\mathrm{Fe}} = \frac{U_{\mathrm{rt}}^2}{P_{\mathrm{Vlr}}} \tag{2.9}$$

The iron current I_{FE} is significantly smaller as compared to the magnetizing current I_{m}. Due to this the main reactance X_{h} will be determined using only the magnetizing current: [4]

$$X_{\mathrm{h}} = \frac{1}{I_{\mathrm{m}}} \cdot \frac{U_{\mathrm{rt}}^2}{S_{\mathrm{rt}}} \tag{2.10}$$

With the use of the previously calculated values and elementary electrical summarizing rules, it us possible to obtain the following equations.

$$\underline{Y}_{\mathrm{A}} = \frac{1}{R_{\mathrm{A}} + \underline{X}_{\mathrm{A}}} \tag{2.11}$$

$$\underline{Y}'_{\mathrm{B}} = \frac{1}{R'_{\mathrm{B}} + \underline{X}'_{\mathrm{B}}} \tag{2.12}$$

$$\underline{Y}_{\mathrm{m}} = \frac{1}{R_{\mathrm{Fe}}} + \frac{1}{\underline{X}_{\mathrm{h}}} \tag{2.13}$$

With $\underline{Y}_{\mathrm{A}}$, $\underline{Y}'_{\mathrm{B}}$ and $\underline{Y}_{\mathrm{m}}$, the circulation in both loops results in [19]:

$$\begin{bmatrix} \underline{I}_{\mathrm{A}} \\ \underline{I}'_{\mathrm{B}} \\ 0 \end{bmatrix} = \left[\begin{array}{c|c|c} \underline{Y}_{\mathrm{A}} & 0 & -\underline{Y}_{\mathrm{A}} \\ \hline 0 & \underline{Y}'_{\mathrm{B}} & -\underline{Y}'_{\mathrm{B}} \\ \hline \underline{Y}_{\mathrm{A}} & -\underline{Y}'_{\mathrm{B}} & \underline{Y}_{\mathrm{A}} + \underline{Y}'_{\mathrm{B}} + \underline{Y}_{\mathrm{m}} \end{array}\right] \begin{bmatrix} \underline{U}_{\mathrm{A}} \\ \underline{U}'_{\mathrm{B}} \\ \underline{U}_{\mathrm{m}} \end{bmatrix} \tag{2.14}$$

Reducing Equation 2.14 by the third line and inserting the transformation factor $\underline{\ddot{u}}$, results in the transformer admittance matrix [19].

$$\underline{\boldsymbol{Y}}_{\mathrm{Tt}} = \frac{1}{\underline{Y}_{\mathrm{A}} + \underline{Y}'_{\mathrm{B}} + \underline{Y}_{\mathrm{m}}} \left[\begin{array}{c|c} \underline{Y}_{\mathrm{A}} \left(\underline{Y}'_{\mathrm{B}} + \underline{Y}_{\mathrm{m}}\right) & -\underline{\ddot{u}}\ \underline{Y}_{\mathrm{A}}\ \underline{Y}'_{\mathrm{B}} \\ \hline -\underline{\ddot{u}}^{*}\ \underline{Y}_{\mathrm{A}}\ \underline{Y}'_{\mathrm{B}} & |\underline{\ddot{u}}|^2\ \underline{Y}'_{\mathrm{B}} \left(\underline{Y}_{\mathrm{A}} + \underline{Y}_{\mathrm{m}}\right) \end{array} \right] \tag{2.15}$$

Line

Over the entire line length, there is an inductive and capacitive linkage. The precise line equation consists of so called distributed parameters. Especially the loop resistance and loop inductance are frequency dependent. While applying the method of symmetrical components, an assumption is made. The frequency will be constant and identical to the utility frequency. This simplifies the line model by changing the concatenation to a constant concentration. [9]

Furthermore, when a lines propagation constant combined with its length is significantly smaller than one ($|\gamma l| \ll 1$), it is considered an electrically short line [4]. Considering utility frequency, almost all lines in the low-voltage grid analysed during this work can assumed to be short lines. Therefore all line models in this work are represented with concentrated parameters.

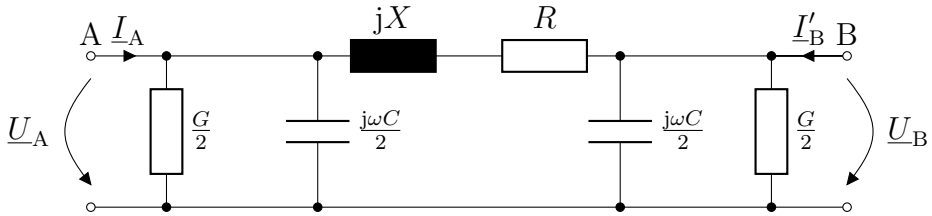

Figure 2.3 Π-equivalent circuit of a line segment [19]

The different segments of the equivalent circuit shown in Figure 2.3 can be depicted as follows [19].

$$\underline{\boldsymbol{Y}}_{\mathrm{A}} = \underline{\boldsymbol{Y}}_{\mathrm{B}} = \frac{1}{2}\left(G + \mathrm{j}\omega C\right) \tag{2.16}$$

$$\underline{\boldsymbol{Y}}_{\mathrm{m}} = \frac{1}{R + \underline{X}} \tag{2.17}$$

By circulation of the central loop the line admittance matrix is set-up [19].

$$\underline{\boldsymbol{Y}}_{\mathrm{Tl}} = \left[\begin{array}{c|c} \underline{Y}_{\mathrm{A}} + \underline{Y}_{\mathrm{m}} & -\underline{Y}_{\mathrm{m}} \\ \hline -\underline{Y}_{\mathrm{m}} & \underline{Y}_{\mathrm{B}} + \underline{Y}_{\mathrm{m}} \end{array}\right] \tag{2.18}$$

2.5 Modeling of Network Topology

The common layout and physical connections between the equipment and the grid are described via the network topology. It is possible to construct a grid using different network topologies as displayed in figure 2.4. LV networks can be connected via a radial, ring or mesh system. Radial networks are characterised by only on connection to upper voltage level (Medium voltage (MV)). Ring networks are generally operated as separated radial network. In case a line fault occurs a switch within the ring network can be closed ensuring a continues supply of power. A grid that is feed by more than one connection to the upper voltage level or via DER and multiple connections within is defined as a mesh network. [3]

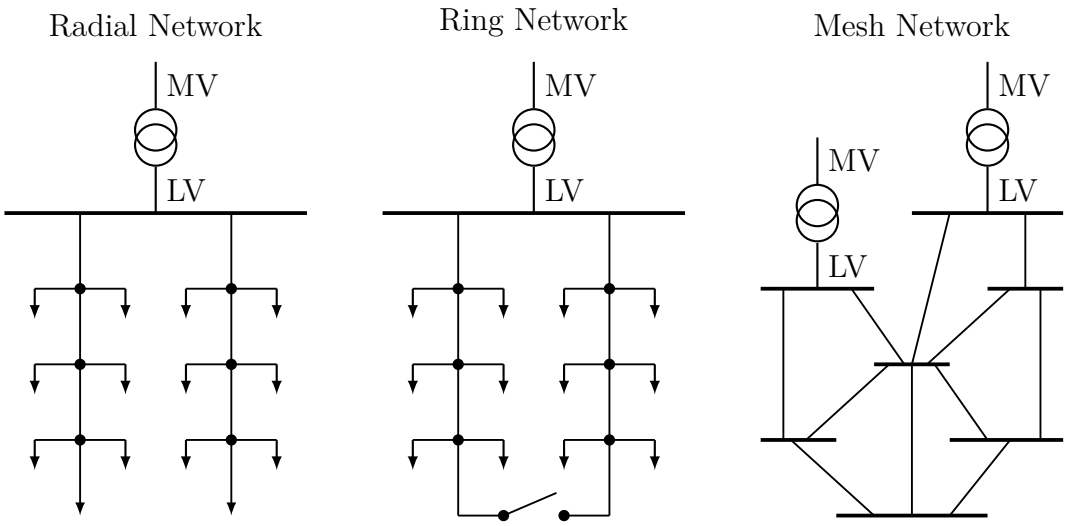

Figure 2.4 LV network topologies [1][3]

The mathematical description of electrical networks is done through nodes and branches, via the network topology. Busbars are considered nodes/connection points between equipment and grid, allowing for the connections or separation of transformers, lines, power generators and consumer loads [3]. The strokes between two connection points, so called branches, can be divided into two categories.

Transformers and lines are regarded as longitudinal elements, while power injection points and consumer loads are lateral elements. Longitudinal elements are between two points/nodes. Lateral elements can only be connected to one node at any time. [34]

This construct of nodes and branches allows for variable interconnections and leads to changeable network topologies. In order to accurately depict electrical grids, the topology has to be reproduced using mathematical analogies.

Nodal-Terminal-Incidence-Matrix

In order to accurately determine the grid topology, terminals are logically assigned to nodes [19]. This linkage of the equipment equations to the grid equation system is done via the Nodal-Terminal-Incidence-Matrix $\boldsymbol{K}_{\mathrm{KT}}$ [10]. Every row inside the matrix is linked to a single node, while every column corresponds to one equipment terminal. The construction of the Nodal-Terminal-Incidence-Matrix elements is done via the following scheme [19]:

- Connections between a terminal and a grid node will me marked with a 1
- The remaining elements will be denoted by 0

Nodal-Admittance-Matrix

The previously established admittance matrix and Nodal-Terminal-Incidence-Matrix are used to calculate the Nodal-Admittance-Matrix $\underline{\boldsymbol{Y}}_{\mathrm{KK}}$. In this sparsely populated matrix, the network equipment, as well as the network topology, are preserved. [10]

$$\underline{\boldsymbol{Y}}_{\mathrm{KK}} = -\boldsymbol{K}_{\mathrm{KT}} \cdot \underline{\boldsymbol{Y}}_{\mathrm{T}} \cdot \boldsymbol{K}_{\mathrm{KT}}^{\mathrm{T}} \tag{2.19}$$

The Nodal-Admittance-Matrix is symmetrical along the diagonal. The identical non-diagonal elements ik and ki display the sum of all admittances between the nodes i and k for all parallel branches a [10].

$$\underline{y}_{ik} = \underline{y}_{ki} = \sum_{a} \underline{Y}_{\mathrm{KK},ik} \tag{2.20}$$

The negative sum of the admittances $\underline{Y}_{i0}$, that are positioned between node i and the reference node 0 and its parallel branches b are placed on the diagonal [10].

$$\underline{y}_{ii} = -\sum_{b} \underline{Y}_{i0} \sum_{n-1} \underline{y}_{ik} \tag{2.21}$$

The Nodal-Admittance-Matrix has the following properties [9]:

- quadratic with the dimensions n x n ($n = k - 1$)
- symmetrical as long as there is no phase-shifting transformer
- sparsely populated
- almost singular, due to $\underline{y}_{ii} = -\underline{y}_{i0} - \sum \underline{y}_{ik}$ for $\underline{y}_{i0} \ll \sum \underline{y}_{ik}$

2.6 Power Flow with Newton-Raphson Method

In order to determine the voltages, currents and power flows inside a grid, so called power flow algorithms are used. By obtaining this information it is possible to determine grid losses and reactive power demands for a steady state scenario. This makes the power flow algorithms indispensable tools for grid monitoring and illustration purposes. [9]

Several different approaches to solve the grid state identification problems are available, e.g. fixed-point (Gauss-Seidel) or tangential (Newton-Rapshon) procedures [18]. Most commonly the Newton-Rapshon method is used, due to its lower amount of iteration steps and optimal convergence characteristics [10]. In this work, the Newton-Rapshon-Method will be applied to solve all power flow problems.

Node Specification

Each grid node must be one of three categories in order to perform power flow calculations. The distinction is made between electrical load nodes (P-Q), generator nodes (P-U) and the slack node (U-δ). [9]
The different node types, together with their known and desired quantity are listed in table 2.1.

Table 2.1 Node Specifications [9]

Node type	known quantity	desired quantity
Generator node	P and U	Q and δ
Slack node	U and δ	P and Q

When applying the power flow algorithm, at least one slack node must be defined. The slack node permits the lateral line and transformer terms to be neglected, which leads to

a non singular Nodal-Admittance-Matrix. Additionally, the slack node must be able to account for the the total power balance. Therefore, big power plants or higher voltage level grid connections should be chosen as slack node. With more than one slack node a power flow between the two slack nodes those will be forced, which complecates accurately describe the grid state [10]

Allthrough it is possible to overcome the forced power flow problem through different methods, it is not necessary for the grid analyzed in this work. The difference compared to other solving methods represented in [27] is only marginal at grid power levels analyzed at in this work.

Generator nodes have a predetermined active power P and voltage U. This is due to most generators being regulated via their power and voltage. However, if the generator is regulated via the active and reactive power, it is possible to treat them as load nodes with negative power flow. [9]

Load nodes are the majority of nodes inside a grid. Depending on the load composition and characteristics, the load nodes can be voltage depend or constant. The active and reactive power and their corresponding voltage dependency can commonly be described with the following exponential equations: [9][8]

$$P = P_0 \left(\frac{U}{U_0}\right)^p \tag{2.22}$$

$$Q = Q_0 \left(\frac{U}{U_0}\right)^q \tag{2.23}$$

The active power exponent p along side the reactive power exponent q indicate the degree of voltage dependency as it can be seen in figure 2.5. Generally those two values are in the range of 0 to 2. [9]
For the power flow calculation of this work, the EVCQ load is assumed to be constant. This results in both exponents being 0.

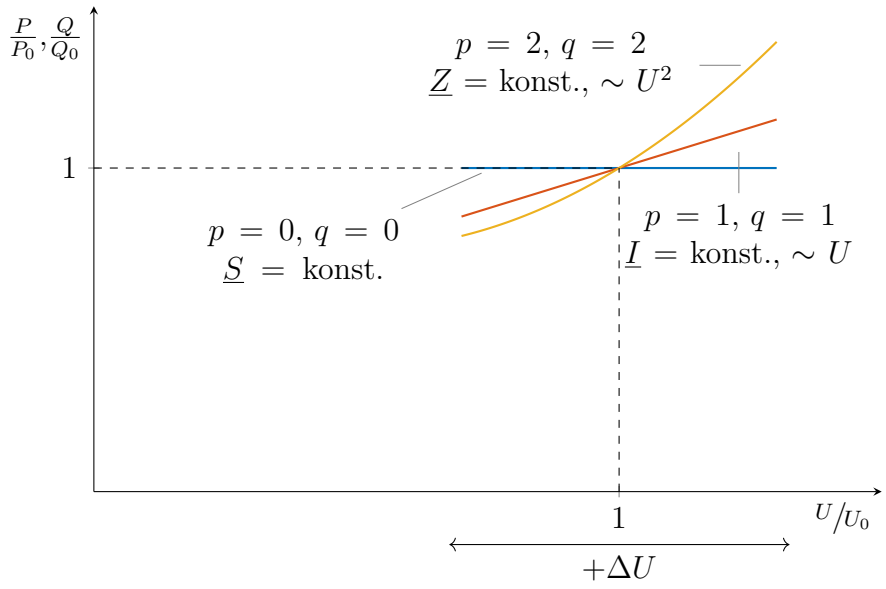

Figure 2.5 Load nodes exponential equation representation [59]

Algorithm

The power flow by Newton-Raphson algorithm is an iterative method for finding the roots [10]. The diagonal matrix $\underline{\boldsymbol{U}}_{\mathrm{K}}$ is constructed using the node voltage vector $\underline{\boldsymbol{u}}_{\mathrm{K}}$. Based on the node voltage equation 2.41 for the grid, the following power equation is created [9]:

$$3\underline{\boldsymbol{U}}_{\mathrm{K}}\underline{\boldsymbol{Y}}^{*}_{\mathrm{KK}}\boldsymbol{u}^{*}_{\mathrm{K}} = 3\underline{\boldsymbol{U}}_{\mathrm{K}}\boldsymbol{i}^{*}_{\mathrm{K}} \tag{2.24}$$

The left side of equation 2.24 describes the flow of power at the nodes between the grid ($\underline{\boldsymbol{s}}_{\mathrm{N}}$), while the right side of the equation describes the power that is injected or removed from the nodes ($\underline{\boldsymbol{s}}_{\mathrm{K}}$). [9]

$$\underline{\boldsymbol{s}}_{\mathrm{N}} = 3\underline{\boldsymbol{U}}_{\mathrm{K}}\underline{\boldsymbol{Y}}^{*}_{\mathrm{KK}}\underline{\boldsymbol{u}}^{*}_{\mathrm{K}} = \boldsymbol{p}_{\mathrm{N}} + \mathrm{j}\boldsymbol{q}_{\mathrm{N}} \tag{2.25}$$

$$\underline{\boldsymbol{s}}_{\mathrm{K}} = 3\underline{\boldsymbol{U}}_{\mathrm{K}}\underline{\boldsymbol{i}}^{*}_{\mathrm{K}} = \boldsymbol{p}_{\mathrm{K}} + \mathrm{j}\boldsymbol{q}_{\mathrm{K}} \tag{2.26}$$

The roots for the active and reactive part of the power flow calculations will be determined separately [8]:

$$\boldsymbol{p}_{\mathrm{N}} = \mathrm{Re}\{3\underline{\boldsymbol{U}}_{\mathrm{K}}\underline{\boldsymbol{Y}}^{*}_{\mathrm{KK}}\underline{\boldsymbol{u}}^{*}_{\mathrm{K}}\} \tag{2.27}$$

$$\boldsymbol{q}_{\mathrm{N}} = \mathrm{Im}\{3\underline{\boldsymbol{U}}_{\mathrm{K}}\underline{\boldsymbol{Y}}^{*}_{\mathrm{KK}}\underline{\boldsymbol{u}}^{*}_{\mathrm{K}}\} \tag{2.28}$$

In order to solve both equations mentioned above, the Taylor-series expansion, with a termination after the first iteration step, is used to close in on the state vector $\boldsymbol{x}_{\nu}$. The state vector is constructed using the voltage angle and magnitude ($\boldsymbol{x} = [\boldsymbol{\delta}^{\mathrm{T}}\ \boldsymbol{u}_{\mathrm{K}}^{\mathrm{T}}]^{\mathrm{T}}$) and changes with each iteration step ν. This results in the following two linearized equations. [10]

$$\left(\frac{\partial \Delta \boldsymbol{p}\,(\boldsymbol{x}_{\nu})}{\partial \boldsymbol{x}^{\mathrm{T}}}\right)\Delta \boldsymbol{x}_{\nu+1} = -\Delta \boldsymbol{p}\,(x_{\nu}) \tag{2.29}$$

$$\left(\frac{\partial \Delta \boldsymbol{q}\,(\boldsymbol{x}_{\nu})}{\partial \boldsymbol{x}^{\mathrm{T}}}\right)\Delta \boldsymbol{x}_{\nu+1} = -\Delta \boldsymbol{q}\,(x_{\nu}) \tag{2.30}$$

The two equation above can be combined into one equation [10]:

$$\begin{bmatrix} \frac{\partial \Delta \boldsymbol{p}(\boldsymbol{x}_{\nu})}{\partial \boldsymbol{x}^{\mathrm{T}}} \\ \frac{\partial \Delta \boldsymbol{q}(\boldsymbol{x}_{\nu})}{\partial \boldsymbol{x}^{\mathrm{T}}} \end{bmatrix} \cdot \Delta \boldsymbol{x}_{\nu+1} = -\begin{bmatrix} \Delta \boldsymbol{p}\,(x_{\nu}) \\ \Delta \boldsymbol{q}\,(x_{\nu}) \end{bmatrix} \tag{2.31}$$

$$\boldsymbol{J}_{\nu} \cdot \Delta \boldsymbol{x}_{\nu+1} = -\Delta \boldsymbol{y}_{\nu} \tag{2.32}$$

The Jacobian matrix $\boldsymbol{J}_{\nu}$ and its submatrices H, N, M, L are constructed using the power equation, with $\boldsymbol{S}_{\mathrm{J}}$ being a diagonal matrix made using the vector elements from equation 2.25 or 2.26. [9]

$$\underline{\boldsymbol{S}}_{\mathrm{J}} = 3\underline{\boldsymbol{U}}_{\mathrm{K}}\underline{\boldsymbol{Y}}^{*}_{\mathrm{KK}}\underline{\boldsymbol{u}}^{*}_{\mathrm{K}} = 3\underline{\boldsymbol{U}}_{\mathrm{K}}\underline{\boldsymbol{i}}^{*}_{\mathrm{K}} \tag{2.33}$$

$$\boldsymbol{J} = \begin{bmatrix} H & N \\ M & L \end{bmatrix} = \begin{bmatrix} \mathrm{Im}\{\underline{\boldsymbol{S}}_{\mathrm{J}}\} - \boldsymbol{Q}_{\mathrm{N}} & \mathrm{Re}\{\underline{\boldsymbol{S}}_{\mathrm{J}}\} + \boldsymbol{P}_{\mathrm{N}} - \boldsymbol{P}'_{\mathrm{K}} \\ -\mathrm{Re}\{\underline{\boldsymbol{S}}_{\mathrm{J}}\} - \boldsymbol{P}_{\mathrm{N}} & \mathrm{Im}\{\underline{\boldsymbol{S}}_{\mathrm{J}}\} + \boldsymbol{Q}_{\mathrm{N}} - \boldsymbol{Q}'_{\mathrm{K}} \end{bmatrix} \tag{2.34}$$

The elements of the diagonal matrices $\boldsymbol{P}_{\mathrm{N}}$ and $\boldsymbol{Q}_{\mathrm{N}}$ are calculated using the following equation [9]:

$$\boldsymbol{p}_{\mathrm{N}} = \sum_{i=1}^{\mathrm{n}} \mathrm{Re}\{\underline{\boldsymbol{s}}_{\mathrm{J,i}}\} \tag{2.35}$$

$$\boldsymbol{q}_{\mathrm{N}} = \sum_{i=1}^{\mathrm{n}} \mathrm{Im}\{\underline{\boldsymbol{s}}_{\mathrm{J,i}}\} \tag{2.36}$$

The matrices $\boldsymbol{P}'_{\mathrm{K}}$ and $\boldsymbol{Q}'_{\mathrm{K}}$ are calculated as follows, with $\boldsymbol{P}_i$ and $\boldsymbol{Q}_i$ are taken from equation 2.22 and 2.23 [9]:

$$\boldsymbol{P}'_{\mathrm{K}} = \mathrm{diag}\,(p_i \boldsymbol{P}_i) \tag{2.37}$$

$$\boldsymbol{Q}'_{\mathrm{K}} = \mathrm{diag}\,(q_i \boldsymbol{Q}_i) \tag{2.38}$$

To kick of the iterative equation 2.32, it is assumed that the state vector equals the initial values, for the first step ($\boldsymbol{x}_\nu = \Delta\boldsymbol{x}_0$). If the starting values are unknown, rated voltage is generally assumed. Combined with the Jacobian matrix it possible to calculate the right hand side ($-\Delta\boldsymbol{y}_\nu$) of equation 2.32. After solving equation 2.32 the state vector is improved by $\Delta\boldsymbol{x}_{\nu+1}$. [10][9]

$$\boldsymbol{x}_{\nu+1} = \boldsymbol{x}_\nu + \Delta\boldsymbol{x}_{\nu+1} \tag{2.39}$$

This iteration loop will be repeated until, there is only a specified difference between two consecutive iterations. The termination criteria can be described by the following equation:

$$\max\left(|\Delta\boldsymbol{x}_\nu|\right) < \varepsilon \tag{2.40}$$

Attaining the termination criteria, the final result calculations will be made. Using the node voltages, $\underline{\boldsymbol{u}}_{\mathrm{K}}$ that has been obtained through the loop, it is possible to determine the node currents [19].

$$\underline{\boldsymbol{i}}_{\mathrm{K}} = \underline{\boldsymbol{Y}}_{\mathrm{KK}} \cdot \underline{\boldsymbol{u}}_{\mathrm{K}} \tag{2.41}$$

Next the terminal powers can be calculated [19]:

$$\underline{\boldsymbol{s}}_{\mathrm{T}} = \boldsymbol{K}_{\mathrm{KT}}^{\mathrm{T}} \underline{\boldsymbol{u}}_{\mathrm{K}} \underline{\boldsymbol{i}}_{\mathrm{K}}^{*} \tag{2.42}$$

In the final step, the grid losses can be calculated as a sum for the vector[19]:

$$\underline{\boldsymbol{s}}_{\mathrm{K}} = \underline{\boldsymbol{u}}_{\mathrm{K}} \left(\underline{\boldsymbol{Y}}_{\mathrm{KK}} \underline{\boldsymbol{u}}_{\mathrm{K}} \right)^{*} \tag{2.43}$$

Figure 2.6 represents the general procedure for power flow by Newton-Raphson algorithm. For smaller networks, like the ones being analysed in this work, the power flow iteration only needs a couple of steps to reach a solution. In case a solution can not be determined within 20 iteration steps the loop will be stopped.

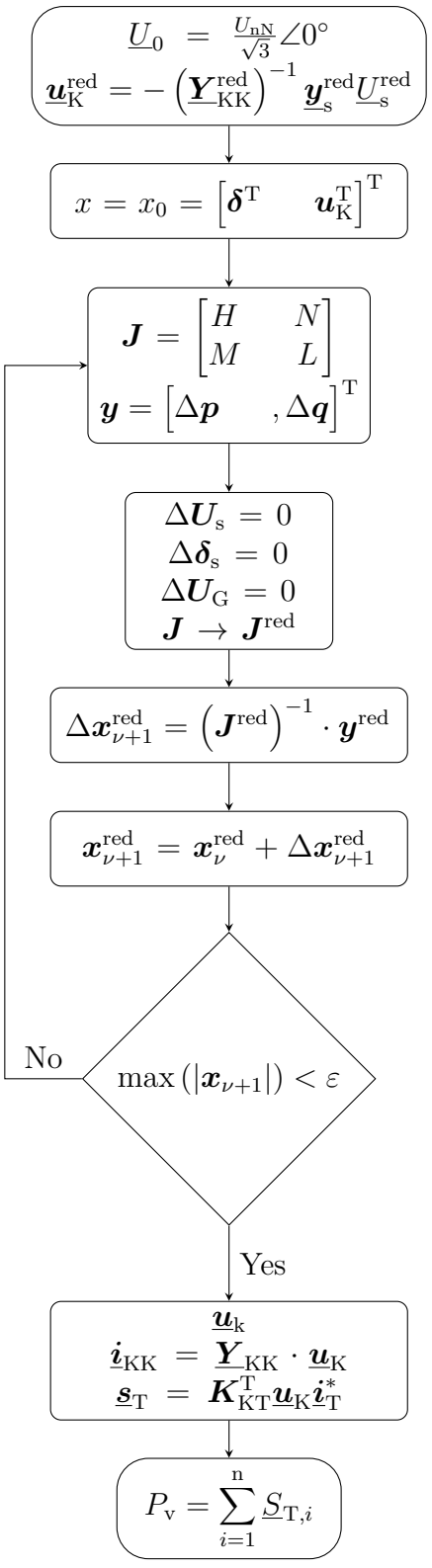

Figure 2.6 Flowchart for the power flow by Newton-Rapshon algorithm [9][10][59] [1]

2.7 Grid Operational Limits

Using power flow calculations, grids and their respective power flows can be determined, but without any guidelines on physical networks, it is not possible to accurately interpret the results. This can be resolved by taking a closer look at grid codes and guidelines.
In order to ensure safe, secure and efficient grid operation, operational strategies and rules must be followed. These rules are specified by the ENTSO-E and are implemented by each grid operator. Every supplier and consumer that is part of the European electrical grid is required to make sure that he is following regulations regarding voltage, frequency and general grid stability. Furthermore, when running or expanding a grid certain norms should be upheld. These norms are guidelines to guarantee that an efficient and safe operation of the grid is achieved at all times. For this work, the grid codes regarding voltage band compliance and norms about current-carrying capacity of lines are most importance and will be discussed further in detail.

2.7.1 Voltage Band Compliance

The voltage band compliance is a vital task to ensure strain relief for the grid and prevent overload of equipment [33]. Before new equipment is installed, the grid must be analysed to determine critical operating points, which could result in voltage violation. According to norm DIN-EN-50160, for steady state, the voltage at any node inside the distribution grid may fluctuate only by ±10 % (0,9 p.u. to 1,1 p.u.) of the rated voltage during normal operation. More precisely, over the period of one year, 95 % of all 10 minute averages must be inside this limit [65][54]. To not fully exhaust the voltage band within the LV grid, the upper voltage band limit is set to 1,05 p.u., while the lower limit is set to 1,0 p.u.. This is done, since the MV grid may already be using +5 % and power injection through private DER, such as Photovoltaic (PV), has the potential to increase the grid voltage further. Because of these unknown know factors the tolerance is created. Whenever these limits are exceeded and optimisation potential is exhausted, grid reinforcement is necessary.

2.7.2 Current-Carrying Compliance

The current-carrying capacity I_{th} limits the maximum permissible current that may flow inside a line without it surpassing its operating temperature and destroying utility. Depending on the type of insulation, ambient temperature, number of strains inside a cable and distance between cables, the current-carrying capacity might be lowered further. [64] This is due to the lines electromagnetic field acting up on other lines near by. In generally the current-carrying capacity is calculated as followed [64]:

$$I_{\mathrm{th}} = I_{\mathrm{r}} \cdot \Pi f \tag{2.44}$$

with I_{r} being the load-capacity and Πf being the conversion factors, to adjust the current rating. Both conversion factors can be found and obtained using DIN VDE 0298-4 [64]. For this work the current-carrying capacity for multiple laid cables next to each other is of interest, since grid reinforcement can be done by laying multiple cables next to each other. As soon as a second cable is laid, with a maximum distance of 7 cm to all other cables, the current-carrying capacity of every cable in its proximity will be reduced [64]. Table 8.5 displays the conversion factor for PVC-cables (NYY, NYCWY) at a ground temperature of 20 °C and a thermal ground resitance of 1 K $\cdot$ m/w [64].

2.8 Sensitivity Index

Grid sensitivity analysis is used to determine the power system response from a single source of influence on all other state variables [37]. This means that, any arbitrary influence and its affect can be depicted, giving valuable information about the relationship of single grid nodes to all others. It is essential to know the grid points, which have the most influence on other nodes, because they are most susceptible to voltage instability [20]. Obtaining this linear dependency of state variable on influencing variables is achieved by linearizing nonlinear system equations at a known operating point [19].

Operating points are known steady system states. All system- and influencing-variables are therefore non-varying and can be achieved through power flow calculation. Commonly, state variable are defined as complex nodal voltages, whereas the influencing variables are all measured values. [19]

Using this information, loads can be placed at the most instable/critical nodes within the network. The placement of loads in such way can also be described as the the worst case scenario. This will result in the most drastic changes within the grid, which are most likely to result in a grid compliance issue.

Grid operators generally care only for the worst possible case, since covering the worst case insures a secure network operation. The worst case can be determined by the most sensitive nodes, thereby only those need to be studied. As a consequence reducing the amount of possible options that need to be analysed.
In contrast, the least sensitive nodes are ideal locations to inject power into the grid, due to their power fluctuation having less effects on other grid nodes.

Information about active and reactive power is only measured at handover locations between grids, power plants or special customers. Typically, the only available information is about magnitudes of currents, voltages and apparent powers. Due to these limitations, the "Nodal currents", "Nodal apparent power", "Active and reactive nodal powers" and "Terminal Values" sensitivity matrix calculation cases have been developed. [19]

Since the active and reactive nodal power is known in this work (chapter 3), the corresponding case is being used and outlined. The nodal apparent power equation (eq. 2.43) is reformed into a function of voltage magnitude and phase angle and linearized at its operating point [19].

$$\begin{bmatrix} \boldsymbol{p}_{\mathrm{K}} \\ \boldsymbol{q}_{\mathrm{K}} \end{bmatrix} \approx \begin{bmatrix} \boldsymbol{p}_{\mathrm{K0}} \\ \boldsymbol{q}_{\mathrm{K0}} \end{bmatrix} + \begin{bmatrix} \Delta\boldsymbol{p}_{\mathrm{K}} \\ \Delta\boldsymbol{q}_{\mathrm{K}} \end{bmatrix} = \begin{bmatrix} \boldsymbol{f}_{\mathrm{PK}} \\ \boldsymbol{f}_{\mathrm{QK}} \end{bmatrix}_{\mathrm{OP}} + \boldsymbol{J}_{\mathrm{PQ}} \begin{bmatrix} \Delta\boldsymbol{\delta}_{\mathrm{K}} \\ \Delta\boldsymbol{u}_{\mathrm{K}} \end{bmatrix} \tag{2.45}$$

thereby the Jacobian is [19]:

$$\boldsymbol{J}_{\mathrm{PQ}} = \left[\begin{array}{ccc:ccc} \frac{\partial P_{\mathrm{K1}}}{\partial \delta_{\mathrm{K1}}} & \cdots & \frac{\partial P_{\mathrm{K1}}}{\partial \delta_{\mathrm{K}n}} & \frac{\partial P_{\mathrm{K1}}}{\partial U_{\mathrm{K1}}} & \cdots & \frac{\partial P_{\mathrm{K1}}}{\partial U_{\mathrm{K}n}} \\ \vdots & \ddots & \vdots & \vdots & \ddots & \vdots \\ \frac{\partial P_{\mathrm{K}n}}{\partial \delta_{\mathrm{K1}}} & \cdots & \frac{\partial P_{\mathrm{K}n}}{\partial \delta_{\mathrm{K}n}} & \frac{\partial P_{\mathrm{K}n}}{\partial U_{\mathrm{K1}}} & \cdots & \frac{\partial P_{\mathrm{K}n}}{\partial U_{\mathrm{K}n}} \\ \hdashline \frac{\partial Q_{\mathrm{K1}}}{\partial \delta_{\mathrm{K1}}} & \cdots & \frac{\partial Q_{\mathrm{K1}}}{\partial \delta_{\mathrm{K}n}} & \frac{\partial Q_{\mathrm{K1}}}{\partial U_{\mathrm{K1}}} & \cdots & \frac{\partial Q_{\mathrm{K1}}}{\partial U_{\mathrm{K}n}} \\ \vdots & \ddots & \vdots & \vdots & \ddots & \vdots \\ \frac{\partial Q_{\mathrm{K}n}}{\partial \delta_{\mathrm{K1}}} & \cdots & \frac{\partial Q_{\mathrm{K}n}}{\partial \delta_{\mathrm{K}n}} & \frac{\partial Q_{\mathrm{K}n}}{\partial U_{\mathrm{K1}}} & \cdots & \frac{\partial Q_{\mathrm{K}n}}{\partial U_{\mathrm{K}n}} \end{array}\right] \tag{2.46}$$

Reducing the Jacobian by the slack node and inverting it will result in [19]:

$$\boldsymbol{B}_{\mathrm{UK,PQ}} = \boldsymbol{J}_{\mathrm{PQ,red}}^{-1} = \left[\begin{array}{c:c} \boldsymbol{B}_{\delta,\mathrm{P}} & \boldsymbol{B}_{\delta,\mathrm{Q}} \\ \hdashline \boldsymbol{B}_{\mathrm{U,P}} & \boldsymbol{B}_{\mathrm{U,Q}} \end{array}\right] \tag{2.47}$$

with the four sensitivity matrices proceeding to the two following [19]:

$$\Delta\boldsymbol{\delta}_{\mathrm{K}} = \boldsymbol{B}_{\delta,\mathrm{P}}\ \Delta\boldsymbol{p}_{\mathrm{K}} + \boldsymbol{B}_{\delta,\mathrm{Q}}\ \Delta\boldsymbol{q}_{\mathrm{K}} \tag{2.48}$$

$$\Delta\boldsymbol{u}_{\mathrm{K}} = \boldsymbol{B}_{\mathrm{U,P}}\ \Delta\boldsymbol{p}_{\mathrm{K}} + \boldsymbol{B}_{\mathrm{U,Q}}\ \Delta\boldsymbol{q}_{\mathrm{K}} \tag{2.49}$$

The resulting sensitivity matrices, when converted from polar to cartesian coordinates, of active and reactive power are equal to the inverse Jacobian from the first iteration step of the load flow calculations using the Newton-Raphson algorithm. For this reason, power sensitivity matrices are not fully accurate, but exact enough for the acceptable grid state identification. [37]

2.9 Load Torque Approach

The load torque approach can be used to detect voltage band violations [16]. Identifying possible violations is important for the network operator since he has to uphold the grid codes set by the ENTSO-E. The load torque approach reveals the influence of a single node on all other nodes, this information can be used to approximate possible voltage band violations. Furthermore, the load torque approach exposes the node's sensitivities and can be used to rate each node. The most sensitive nodes will have a higher rating and thereby have a larger affect on all other nodes within the grid.

Generally, voltage band violations are more common in long grids with few interconnections. Rural and suburban grids meet all these conditions and are typically dealing with voltage problems instead of overloaded equipment. The voltage drop is caused by the line impedances. [35]

Typically, iterative algorithms must be used to calculate the grids voltages and power flows, but in low and medium voltage grids, that are radial or ring connected, it is possible to use simplified calculation methods. These methods allow to calculate the nodes that have the largest leverage onto the grid.
Like previously mentioned, all lines in the network are considered electrically short lines ($|\gamma l| \ll 1$). As a consequence, the vertical elements in the lines Π-equivalent circuit (see figure 2.3) can be neglected in MV and LV networks, due to them being much larger than the horizontal resistance and inductance, resulting in a more simplified equivalent circuit. Therefore, only the loop resistance and inductance is used for calculations, whereby the horizontal impedance is greater than its resistance is ($^R/_X \geq 1$). [5][4]

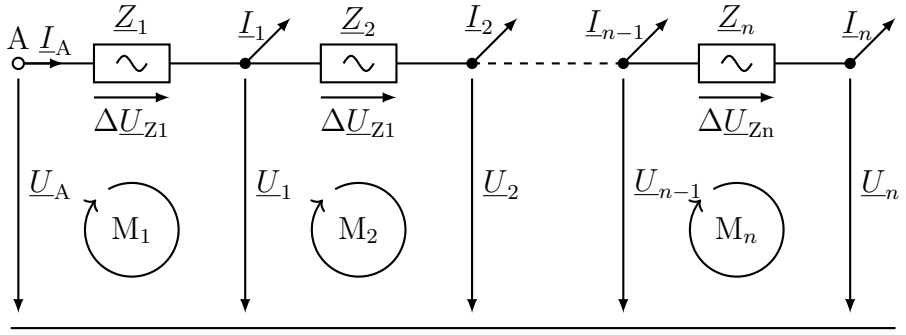

Figure 2.7 Simplified equivalent circuit one-side feed line with multiple consumers [5]

Figure 2.7 displays a simplified equivalent circuit, for a line with only one supply source. However, consumer loads have various ways of being represented, such as constant impedance, constant current, constant power or nonlinear voltage dependencies. Therefore, an iterative calculation method should be used to accurately display such loads.
Generally, there is a lack of knowledge about each individual load inside a grid, so consumer loads are commonly represented using simultaneity factors (section 2.3). Based on known grid information, such as number of households, commercial buildings etc., typical power factors can be applied to consumer loads. [5]

The network used during this work (see chapter 3) specifies the loads and its representation as constant power. Furthermore, the power factors given for each load. As a result, of the small phase angle between the voltage at the beginning and end of the line, it is possible to disregard the imaginary voltage drop [5].

$$Z_{\varphi \mathrm{i}} = l_i \ \left(R'_i \cos(\varphi_i) + X'_i \sin(\varphi_i)\right) \tag{2.50}$$

Using the Kirchhoff's laws and applying it to figure 2.7 will result in n number of equations that will be depicted using matrices. [5]

$$\begin{bmatrix} U_1 \\ U_2 \\ \vdots \\ U_{\mathrm{n}} \end{bmatrix} = \begin{bmatrix} U_{\mathrm{A}} \\ U_1 \\ \vdots \\ U_{\mathrm{n}-1} \end{bmatrix} - \begin{bmatrix} Z_{\varphi 1} & Z_{\varphi 1} & \cdots & Z_{\varphi 1} \\ 0 & Z_{\varphi 2} & \cdots & Z_{\varphi 2} \\ \vdots & \ddots & \ddots & \vdots \\ 0 & \cdots & 0 & Z_{\varphi \mathrm{n}} \end{bmatrix} \begin{bmatrix} I_1 \\ I_2 \\ \vdots \\ I_{\mathrm{n}} \end{bmatrix} \tag{2.51}$$

The maximal voltage drop ΔU_{An} from terminal A to node n using the above mentioned simplifications will result in [5]:

$$\begin{aligned}
\Delta U_{\mathrm{An}} = \;& U_{\mathrm{A}} - U_{\mathrm{n}} \\
= \;& Z_{\varphi 1} \quad (I_1 + I_2 + \cdots + I_{\mathrm{n}-1} + I_{\mathrm{n}}) \\
& + Z_{\varphi 1} \quad (I_1 + I_2 + \cdots + I_{\mathrm{n}-1} + I_{\mathrm{n}}) \\
& + \cdots \\
& + Z_{\varphi \mathrm{n}-1} \quad (I_{\mathrm{n}-1} + I_{\mathrm{n}}) \\
& + Z_{\varphi \mathrm{n}} \quad (I_{\mathrm{n}})
\end{aligned} \tag{2.52}$$

In order to use this calculation method for other grids that split up in multiple branches, it is necessary to relocate the branch currents to the intersection point to reduce the grid to one single string. Afterwards, single branches can be split up again to repeat the procedure till all node voltages have been identified. [5]

2.10 Monte-Carlo Simulation

The Monte Carlo method provides an option to represent uncertain parameters. Using the underlying concept of randomness, the method tries to approximate the solution through probability distribution. During a Monte Carlo simulation, the same simulation is repeated multiple times using different input parameters. Each simulation cycle can be described as one iteration ν. The input values are chosen based on an estimated range of values instead of fixed values. The randomly picked values during each iteration are influenced by their probability density. Therefore, the accuracy of the Monte Carlo method itself increases the more values are provided for a given input.
In the scope of power system engineering the Monte Carlo method can be used to estimate the likelihood of critical grid states. The meaningfulness of results can be increased with a greater number of iterations. Consequently, it is essential to find a suitable compromise between accuracy and computing time.

Like mentioned above, the selection of the input values is based on their individual probability density. The probability density can be described using various models (Weibull-, Gamma-, Gauss-distribution etc) [13]. A normal Gauss distribution is displayed in figure 2.8, with the mean μ at the center of the bell curve and a standard deviation σ.

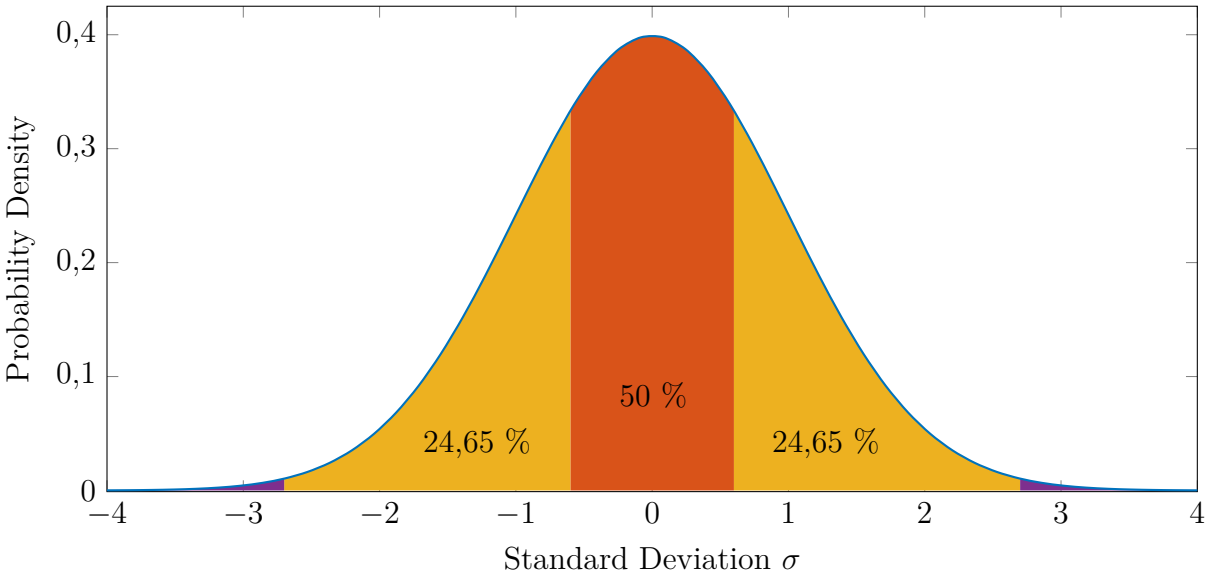

Figure 2.8 Normal Gauss distribution

The three colored areas in figure 2.8 mark the likelihood, that any piece of data will be placed within it. The division displayed in figure 2.8, of the bell curve is also known as Interquartile range (IQR). The probability density function for a Gauss distribution can be described as follows [7].

$$f(x) = \frac{1}{\sqrt{2\pi} \cdot \sigma} \cdot e^{-\frac{(x-\mu)^2}{2\sigma^2}} \tag{2.53}$$

With the mean μ being.:

$$\mu = \frac{1}{\nu} \cdot \sum_{i=1}^{\nu} x_i \tag{2.54}$$

The standard deviation, also referred to as variance, gives information about the spread of data. It is calculated by comparing each value to the mean.

$$\sigma = \sqrt{\frac{1}{\nu} \cdot \sum_{i=1}^{\nu} (x_i - \mu)^2} \tag{2.55}$$

For every uncertain parameter during a Monte Carlo simulation, a distribution function needs to be defined. In this work, only the Gauss distribution is used to represent cable temperature uncertainties (section 4.3).

3 Case Study

This chapter aims to set the general framework for the grid development algorithm. As a foundation, a benchmark network is selected. Subsequently, the current grid state will be analysed to set a baseline for future comparisons. Furthermore, assumptions to the electric vehicle charging infrastructure are made. During this, the power demand of EVCQ within the grid will be determined. To finish off the framework, the costs for grid reinforcement in regard to the benchmark network are presented. This includes a cost investigation for conventional grid reinforcement and more innovate ways such as lihtium-ion storage or CHP.

3.1 Benchmark-Network

In the scope of this work, the Cigre-Benchmark network is investigated. The network was developed to establish a common base for testing the integration of Smart-Grid technologies and future development strategies. Cigre tries to describe the full power system and its underlying networks as accurately as possible. All three voltage levels (High voltage (HV), MV, LV) display an accurate network topology, which can be used for testing purposes. The topology of the HV transmission network has been relatively well defined, while characteristics of the MV and LV distribution grid can vary significantly based on the geographical location. Nevertheless do all networks represent a suitable collection for benchmarking the network side. [53]
For this work only the European low voltage network, in particular the residential sub-network (see figure 3.1) will be examined. This is due to the majority of electric vehicle charging accruing at home [22][26][23].

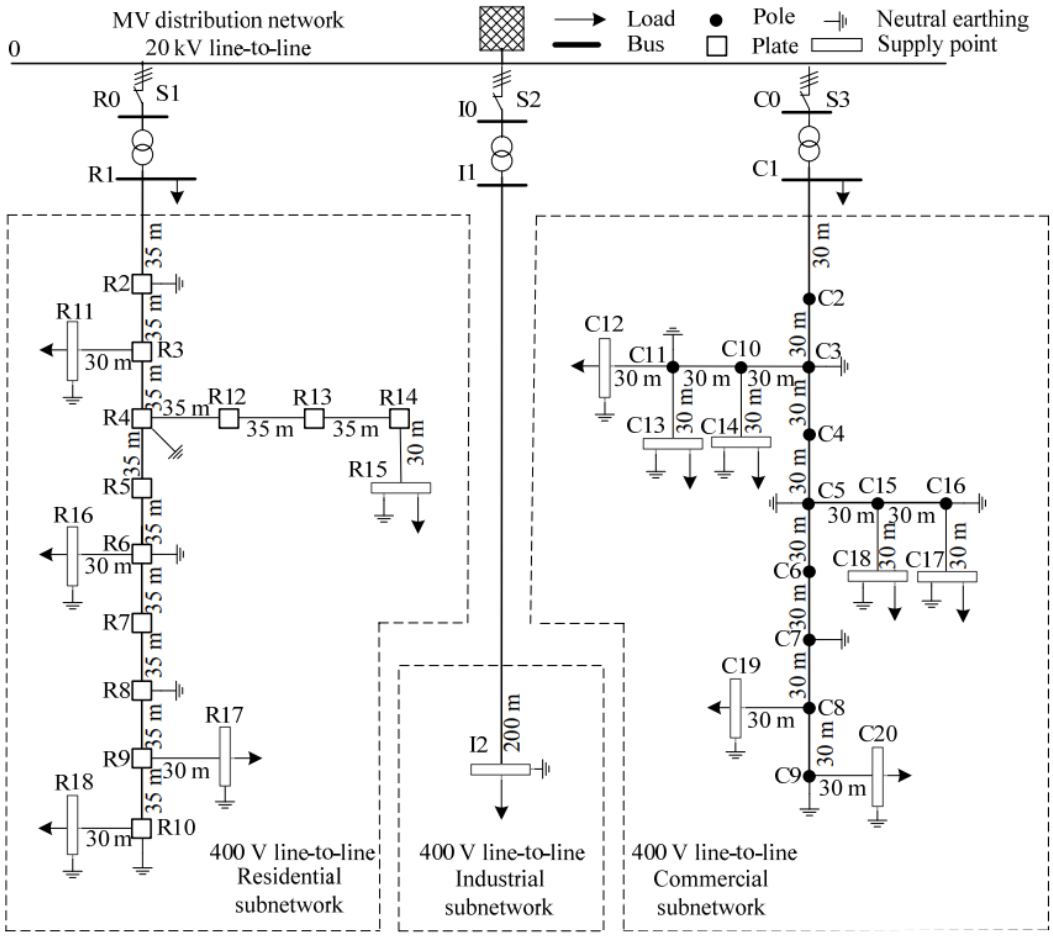

Figure 3.1 Topology of European LV distribution network benchmark [53]

The cigre European LV distribution network uses a balances approach to cover common structural, symmetry, line type and grounding configurations. In Europe the system frequency is 50 Hz. Typically LV distribution networks originate from a MV/LV transformer. The radial structure of such networks may be a combination of one or multiple lines, with consumers connected anywhere along them. The consumers are connected via one of two line types; underground cables, that are primarily used in urban areas with high load density, or overhead cables, which are mainly found in rual areas with comparatively low load density. The grounding for the residential subnetwork is according with IEC 60364. Most commonly TN type or TT type grounding can be found in public LV networks. [53]

Generally LV networks are unbalanced due to the connection of single-phase consumers, although attempts are made using various technologies to reduce this [30][28]. During LV network design, it is common to assume that all phases are balanced, since maximum residential costumer loads are modelled conservatively, thus allowing for a degree of imbalance [68]. In the scope of this work, phases are assumed to be balanced.

The LV residential sub-network, is hooked up via a 500 kVA transformer to the MV grid. Within the sub-network single underground cables are used (see table 8.2). The

underground cables are placed approximately 0.9 m below the surface [53]. Consumer loads are placed along the lines according to table 8.3. Only the total load at each node inside the network is specified. Therefore, every node can be seen as an aggregation of sub-branches with an unspecified number of households attached to it. An investigation into the approximate number of households for each node with a load attached to it will be done in section 3.3.2.

3.2 Reference Benchmark System State

Using the information mentioned above, the current grid state for the residential sub-network can be determined. The power flows at hand set the starting point for any investigation. The voltages present at each node within the cigre benchmark network are displayed in figure 3.2. Due to the radial structure of the grid and no power injection at any node (such as PV or additional MV to LV transformers connections) the voltage levels are all below rated voltage.

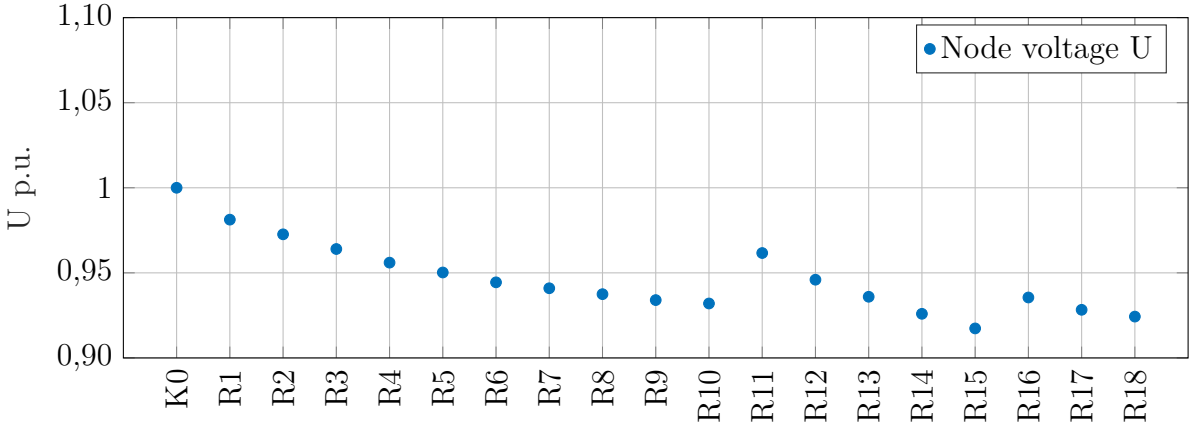

Figure 3.2 Cigre Benchmark network, residential sub-network node voltages

The individual lines in the residential sub-network are connected to the nodes according to table 8.1. The base utilization of each line is displayed in figure 3.3. The transformer degree of utilization is 84,64 %. The combined line utilisation of the residential subnetwork is 55,49 %.

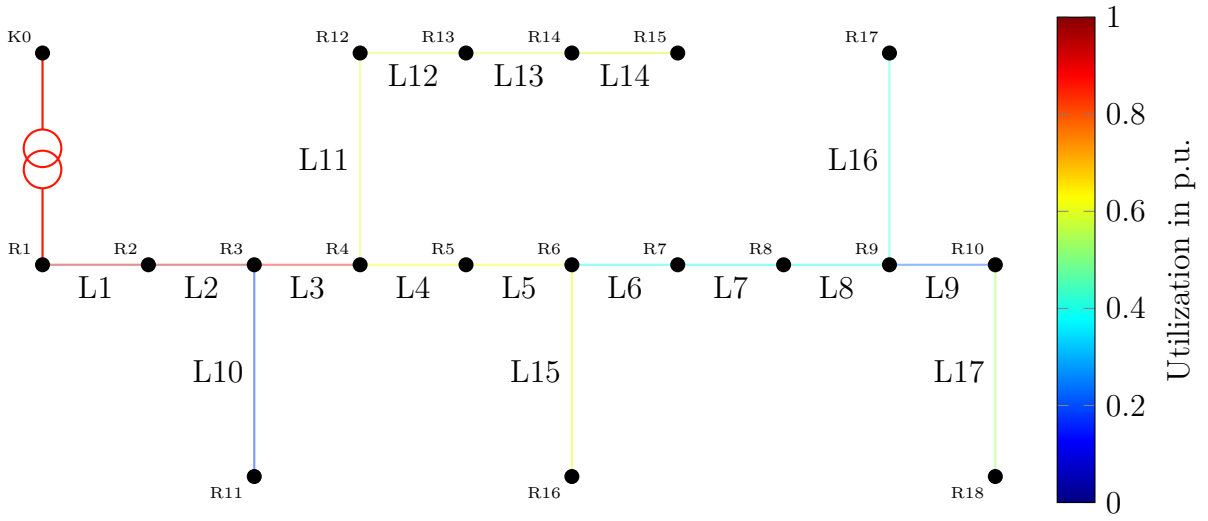

Figure 3.3 Cigre benchmark network, residential sub-network line utilization

3.3 Charging Infrastructure

In order to accurately integrate EVCQ into a grid, the power per equipment and the amount to be incorporated needs to be determined. This section aims to consolidate the various options of EVCQ on the market into one charging unit. Furthermore, the number of households in the grid, together with the current government goals aims to estimate the number of EVCQ, needing to be placed within the grid.

3.3.1 Charging Units

There are various electric vehicle on the market, with different charging specification that need to be accounted for. Generally, there are three different types of chargers, one, two, three phase and DC charging [2]. In order to better represent the different charging types there will be a conversion to "charging units".
Most electric vehicle charging is done at home or in residential areas [15]. To setup electric vehicle chargers DIN 19015-1 and DIN VDE 0100-722 must be considered. The charger should ideally be connected to the breaker box via 3 phases and include a neutral and protective earth wire, with the cables being able to handle at least 32 A. [56]. Additionally, using the emergency charger, an electric vehicle can also be connected to a standard outlet, without the use of a wall box. Electrical outlets for residential dwelling are protected via 16 A fuse [66]. Therefore, the lowest charging power can be achieved by using a single phase outlet, which can draw up to 3,68 kW. To gain a small safety buffer and handle slight variations, one charging unit will be defined as 3,7 kW. By taking multiples of this charging unit, different types of common charging power can be achieved (7,4 kW, 11 kW,

22 kW etc.). Furthermore, the electric vehicle charging units (EVCUs) are assumed to draw only active power, since EVCQs have good power factors even under base loads [29].

3.3.2 Number of Households

The cigre benchmark network gives little information about the number of individual consumers within the grid. Only the total power draw at certain nodes is given (see table 8.3). Using the simultaneity factor equation 2.4, the number of households n_{WE}, dependent on the maximum power draw and convergency factor can be determined for the cigre benchmark network. The results for all combinations (based on table 8.4) can be seen in table 3.1. The average overall maximum power draws, for both convergency factors, has been calculated for each node and rounded down. This average rounded down number of households will be used for future assumption inside this work.

Table 3.1 Number of household at each node dependent on Max. power draw convergency factor

	Node	R1	R11	R15	R16	R17	R18
Max. power draw	convergency factor	Number of households at each node					
5	0,15	231,24	9,15	50,74	54,29	30,97	44,87
	0,2	175,44	7,61	39,38	42,06	24,36	34,93
8	0,12	171,38	4,29	33,78	36,41	19,27	29,43
	0,15	138,88	3,91	28,12	30,25	16,32	24,59
30	0,06	61,66	0,06	4,56	5,28	1,41	3,45
	0,07	54,40	0,07	4,34	5,01	1,39	3,32
15	0,7	17,22	0,94	4,10	4,36	2,62	3,66
18		14,25	0,73	3,34	3,56	2,12	2,98
Average round down		108	3	21	22	12	18

3.3.3 Penetration of Charging Infrastructure

An almost quadratic increase in electric vehicle can be observed in figure 3.4. The development in electric vehicles [62] and their charging needs are transitioning the current energy demands. Because of the current changes in automotive industry, only vague prediction for the near future can be made. In 2011 the German government introduced the electrical mobility program, which had the goal to increase the amount of electric vehicles to six million by 2030 [50]. This program was revised 2020, to have up to 10 million cars by 2030 [52]. Meaning that by the end of the decade at least 20 % of private cars should be electric, when taking the average number of cars per household and person into account. [52][62].

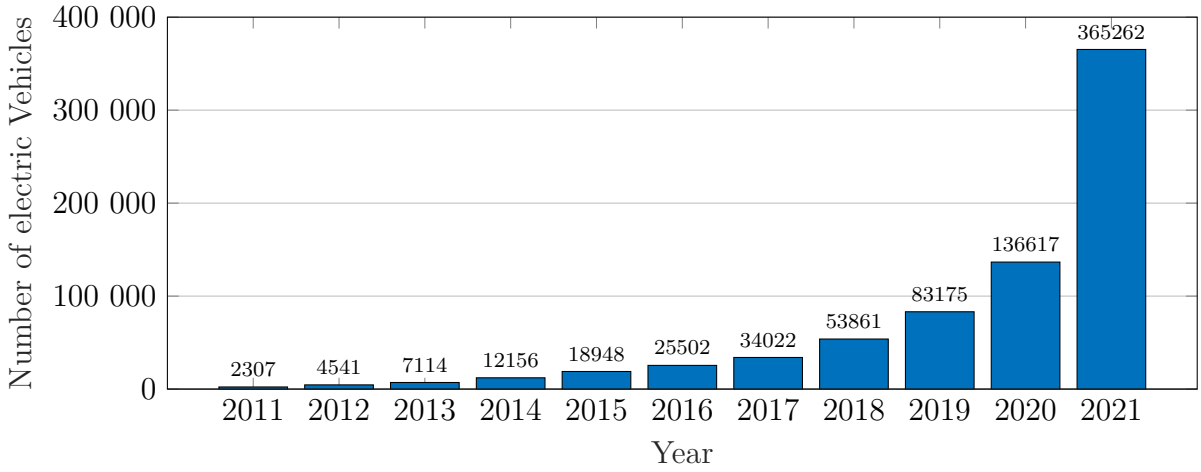

Figure 3.4 Number of electric vehicle in Germany between 2011 and 2021 [61]

Considering the current car registrations and the increase over the years, three scenarios A, B & C, with different amount of electrical vehicle penetration have been advised. For the fist scenario "A", 5 % of all households in the grid are assumed to have one charging unit. In the second scenario "B", this will be increased to 10 % and in the third scenario "C" 20 %. To achieve the current government goals, expansion scenario C needs to be reached.

3.4 Grid Reinforcement Costs

The scope of this section is to model the cost, in order to make cost assumptions, that can be used to analyse different grid reinforcement variants. For better clarification the cost to reinforce the grid will be divided into the following four categories:

- Transmission network (cables & overhead lines)
- Labor cost
- Equipment/Machinery cost
- Associated equipment (transformers)
- DER

The are two options to connect nodes inside a grid; via overhead lines or underground cables. In todays grid overhead lines are a rare sight, even in rural areas. Figure 3.5 shows, that over the last decades more overhead line have been replaced by underground cables. This trend is only going to continue, since the government actively supports this change [50]. This is mostly due to the low acceptance regarding the visual appearance

and lightning protection, even through the cost of overhead lines is roughly three times smaller than underground cables [55]. For this reason, the primary focus for all cost is concerning underground cable installation. This is also in line with the cigre benchmark network model.

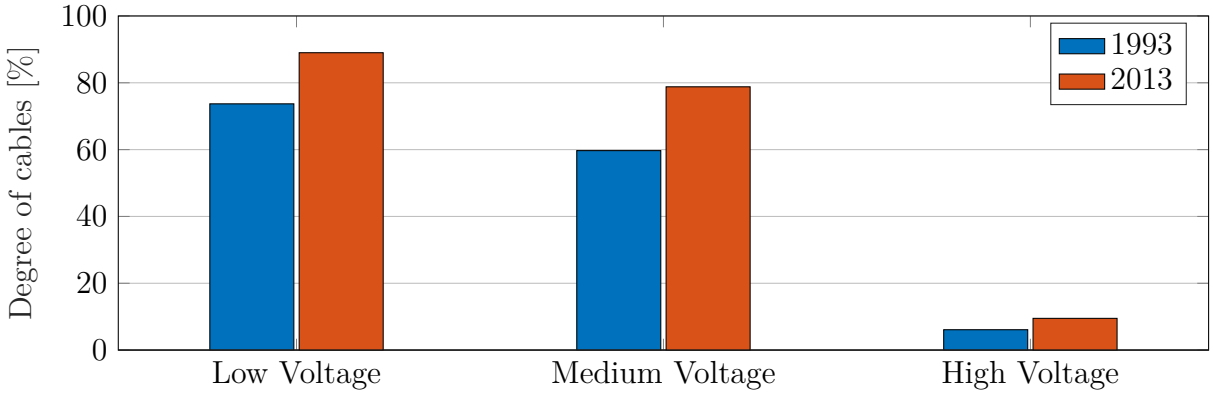

Figure 3.5 Amount of underground cable within the German electricity gird between 1993 and 2013 [57]

When estimating underground grid reinforcement cost, grid operators differentiate between four ground surfaces.

1. Grass/Soil
2. Gravel
3. Pavement
4. Asphalt

The general division between those surfaces is 1. 50 %, 2. 30 %, 3. 10 % and 4. 10 %. Even though this seems incorrect with many streets and sidewalks, there is often a small grass area dividing the cars from the pedestrians, or a buffer zone to the properties. Only in downtown areas the grass/soil portion decreases, while the other proportionally increase. For this work the above mentioned allocation is kept, for the following calculations. [60]

Transmission network

The transmission network cost k_{T} includes the cost regarding the cables itself. The cable price k_{cable} is closely related to the copper/aluminum prices. An increase in those prices will be reflected in an increased cable cost. The insulation cost stays mostly constant. Both cable insulator and copper cost increase quadratically with the cable diameter.
When laying cables, waste from clippings naturally occurs. To account for this, companies typically purchase 3 % more cable than is actually needed. When cables branch off ,or

two ends need to be connected, the cables need to be sleeved together. Because the exact numbers of couplings is unknown before laying the cable it has to be approximated. In general a cost 5€ per meter can be presumed, when braking down the typical length, cost and number of couplings in a project ($k_{\text{coup}} = 5$ €/m). [60]

$$k_{\text{T}} = (k_{\text{cable}} \cdot 1.03 + k_{\text{coup}}) \cdot l \cdot n_{\text{cables}} \tag{3.1}$$

Labor cost

For the laying of cables various amount of subtasks are required. If no conduit has been previously installed ,or it is already full, a trench needs to be dug over the entire length of the line. There are other methods to avoid the need for trenches such horizontal drilling, but this is only used to overcome special obstacles like rivers. Because the cost for horizontal drilling is much grater than regular cable laying, it is only used if no other option is available. Therefore, horizontal drilling will not be considered.
On average every 100 meters an extra assembly pit should be excavated to sleeve cables for branches. In the end, the pits and trenches must be filled again, and the surface must be reconstructed. The cost of all these subtasks depend on the type of surface and cable that where previously installed [60]. For the cigre benchmark network (see Chapter 3.1) it is presumed, that there are no conduits installed. Meaning that a more costly approach is being analysed. Using the general ground surface division as mentioned above will result in the following labor cost [60]; which is split between a fixed cost and a fluctuating cost, that is dependent on the number of cables being installed.

$$k_{\text{L}} = (136,50 \text{ €/m} + 15,50 \text{ €/m} \cdot n_{\text{cables}}) \cdot l \tag{3.2}$$

Equipment/Machinery cost

The equipment cost k_{E} includes all the equipment that is necessary to complete the job, such as truck, excavators, milling machines and other tools. This cost is mostly dependent on the work area and the surface circumstances. Accounting for the general distribution of surfaces worked up on, will result in roughly 5 % of the entire project cost (or 7€ per m) [60].

$$k_{\text{E}} = 7 \text{ €/m} \cdot l \tag{3.3}$$

Associated equipment

In the scope of grid reinforcement, transformers are considered associated equipment [55]. A normal transformer building can house up to one transformer size larger, then installed

at the initial construction. Roughly 50 % of transformers in LV grids are older than 40 years, and about 10 % are older than 50 years [16]. This means that, about half of all transformers should be replaced within the next 10 years. These results have been made by analysing approximately 200 low voltage networks, during the research project e-Home [63] and others [16].
Because of the age of the transformer it is assumed that the current transformer inside the building has not been upgraded; therefore leaving room to house one larger class of transformer. In case the transformer has to be upgraded by an additional size, a new building needs to be constructed, which results in additional cost. Adding up the transformer cost and if necessary the building cost from table 8.8 the total associated equipment cost k_{a} can be determined.

Energy storage system

The acquisition cost k_0 of an energy storage system covers the one time cost for the construction and commissioning. This cost k_0 depends on the necessary storage capacity (kWh) or storage power (kW) or on both. Generally, lithium-ion battery storage system cost revolve around the required capacity cost k_{cap} [12]. The average capacity cost for lithium-ion storage systems is predicted to be 350 €/kWh in 2025 [14]. The required time t, for the storage unit to be able to supply power is assumed to be 8 h.

$$k_0 = P \cdot t \cdot k_{\mathrm{cap}} \tag{3.4}$$

The operational cost k_{oper} is the reoccurring cost over the lifetime t_{use}, of an energy storage system. It is feasible to 2 % of the acquisition cost as the yearly operational cost. [12]

Since the acquisition cost can be written off by the grid operator over the lifetime of the energy storage system, the annuity factor needs to be considered. The annuity factor reflects the initial investment cost for the energy storage system, in relationship to the interest rate i_{rate}. Commonly the interest rate is about 5 % and the maximum lifetime t_{use} for lithium-ion batteries is 20 years [12][14]. Using both variables the annuity factor A can be calculated according to the following equation [12].

$$A = \frac{i_{\mathrm{rate}} \cdot (1 + i_{\mathrm{rate}})^{t_{\mathrm{use}}}}{(1 + i_{\mathrm{rate}})^{t_{\mathrm{use}}} - 1} \tag{3.5}$$

When constructing a storage system the required land should be purchased. For this work the property cost k_{prop} is assumed to be the same as the property cost for a new transformer building, which is approximately 15 000 € [16]. Using the information above

the total storage cost dependent on the lifetime can be calculated.

$$k_{\text{Sto}} = (k_0 \cdot A + k_{\text{oper,Sto}}) \cdot t_{\text{use}} + k_{\text{prop}} \tag{3.6}$$

Combined heat and power

The acquisition cost k_0 of CHP covers the one time cost for the construction and commissioning. This cost k_0 depends on the required electrical power (kW), that should be generated. With a greater electrical power need, the individual cost per kWh decreases. Based on the data in [43] an investment cost function for CHPs, in the range of 5 kW to 2000 kW, was developed.

$$k_0 = \left(8921 \cdot P^{-0,5495} + 276,9\right) \cdot P \tag{3.7}$$

As with energy storage units, the acquisition cost for CHP can be written off by the grid operator, over the lifetime of the CHP. The Annuity factor for its lifetime can be calculated using equation 3.5. According to the German ministry of finance the average useful life for a CHP is 10 years [41]. The interest rate and the property cost are the same as the energy storage system. The operational cost k_{oper} of CHP depends on its operational hours and the kind of maintenance. Total maintenance cost is generally in the range of 0,032 - 0,05 €/kWh$_{\text{el}}$ every year [39]. To be on the safe side, a more costly approach of 0,05 €/kWh is chosen for this work. The total cost of a CHP over its lifetime can therefore be calculated using the following equation.

$$k_{\text{CHP}} = (k_0 \cdot A + k_{\text{oper,CHP}}) \cdot t_{\text{use}} + k_{\text{prop}} \tag{3.8}$$

Total cost

Adding up all the necessary separate cost factors mentioned above will result in the total grid reinforcement cost.

$$k_{\text{total}} = k_{\text{T}} + k_{\text{L}} + k_{\text{E}} + k_{\text{A}} + k_{\text{Sto}} + k_{\text{CHP}} \tag{3.9}$$

4 Preinvestigation

Before the algorithm, a preinvestigation into the case study grid is conducted. This is done to reduce the number of possibilities the algorithm has to account for, thereby reducing the computational effort, while maintaining precision. First, the individual nodes within the grid are being examined regarding their applicability for EVCQ and distributed power generation. Furthermore, the benefit gained through variable transformers related to the chosen scenarios is evaluated. This is concluded by an assessment of possible gird uncertainties, which could influence the results.

4.1 Node Selection

Each node inside the grid has the potential for electric vehicle charging infrastructure or distributed power generation. Therefore, every node could be analysed and simulated individually. This would results in an increase in possibilities, which would only continue to grow with the number of nodes inside the gird. Depending on the computational power and time that is available, it might be feasible to calculate each node individually. Generally, simpler methods are received better, due the decrease in computational work, that would otherwise be required. A deeper investigation into the node selection process can therefore lead to a decrease in node options, while still sustaining accuracy regarding overall grid stability.

Considering the above and the distinct effect each node has on all the other nodes, a wide range of optimization problems are possible. One method, to determine the effect of a single node on all others is the load torque approach. Using this method, the nodes individual leverage on the whole grid (see section 2.9) can be determined. By determining the leverage for every node a ranking can be created. The ranking for every node in the residential subnetwork of the cigre benchmark network can be seen in table 4.1. The node with the highest leverage, will apply the highest total change in voltage in the grid. Therefore, voltage band violations are more prone to accure at the most sensitive node Therefore, when placing consumers or produces at the most sensitive node, will most likely lead to voltage band violation.

Table 4.1 Load Torque Approach Node Sensitivity

Least Sensitive ⟶																Most Sensitive
R1	R2	R3	R4	R5	R6	R11	R7	R8	R12	R9	R16	R10	R17	R13	R18	R14	R15

An alternative approach to find the most vulnerable nodes inside the network is the sensitivity matrix (see section 2.8). Using this method four sensitivity matrices can be

generated. To evaluate the influence of a single node on all others, the sum of each sensitivity matrix row is generated. This leads to four sensitivity vectors, the angle or voltage depended on the active or reactive power. The results from least sensitive to most sensitive node are show in table 4.2.

Table 4.2 Sensitivity Matrix Approach, from least to most sensitive

$\frac{d\Delta\delta}{d\Delta P}$	$\frac{d\Delta\delta}{d\Delta Q}$	$\frac{d\Delta U}{d\Delta P}$	$\frac{d\Delta U}{d\Delta Q}$
R1	R1	R1	R1
R2	R2	R2	R2
R3	R3	R3	R3
R11	R11	R11	R11
R4	R4	R4	R4
R5	R5	R5	R5
R6	R6	R12	R12
R7	R7	R6	R6
R8	R16	R16	R16
R16	R8	R7	R7
R9	R9	R8	R13
R10	R10	R13	R8
R17	R17	R9	R9
R12	R18	R10	R10
R18	R12	R17	R17
R13	R13	R14	R14
R14	R14	R18	R18
R15	R15	R15	R15

During this work EVCQ and DER are assumed to only draw/supply active power. Therefore, only the column with the voltage dependent on the active power (see table 4.2) is further examined. This is due to the voltage band violation being the only one considered. Should the angle also be taken into account, both angle and voltage dependency on active power results need to be combined.

Comparing the third column from table 4.2 to table 4.1, only minor differences can be observed. A direct lineup between those two approaches is displayed in table 4.3. Comparing those two rankings a maximum deviation of three slots can be observed. Only the first three nodes of the residential subnetwork stay the same. These three nodes are the closest to the transformer and have no secondary lines branching off, and are therefore the least sensitive to grid fluctuations. For this work the node order from the sensitivity matrix $\left(\frac{d\Delta U}{d\Delta P}\right)$ is being adopted.

Table 4.3 Load Torque Approach compared to Sensitivity Matrix $\frac{d\Delta U}{d\Delta P}$

Approach	Grid Nodes																	
Load Torque	1	2	3	4	5	6	11	7	8	12	9	16	10	17	13	18	14	15
Sensitivity Matrix	1	2	3	11	4	5	12	6	16	7	8	13	9	10	17	14	18	15
	Least Sensitive $\longrightarrow$ Most Sensitive																	

4.1.1 Nodes for Electric Vehicle Charging Units

The placement of EVCU has a significant impact on the grid state. A random placement of EVCU could consequently lead in an optimal placement, and therefore an unrepresentative cost result. Typically network operators are most interested in the worst case scenario. The most sensitive grid nodes having the greatest impact on the grid and being the most likely to cause grid violations. Therefore placement of loads at these nodes is assumed to be the worst case.

Considering only the most sensitive nodes, allows to cut down on the amount of possibilities, that need to be taken into account. For this work, only the three most and least sensitive nodes are being analyzed to be used to integrate EVCU. According to table 4.3, the three least sensitive nodes are R1, R2, R3, while the three most sensitive nodes are R15, R18, R14. By comparing the cost of the "best" and "worst" case scenario, the maximum occurring cost fluctuation in the benchmark network can be identified. It should be reasonable to assume, that the cost for integrating EVCU at other nodes, is in between the cost for the best and worst possible location. To affirm this theory, the EVCU are integrated concentrated and distributed over all three nodes.

4.1.2 Nodes for Distributed Power Generation

In order to integrate distributed power generation methods most effectively, it is essential to choose nodes which are suited to absorb deviations from the worst case scenario. One could implement power generation at the three nodes, used to integrate of electric vehicle charging infrastructure. This would resolve the problem of further grid expansion for the time being. The drawback would be a power generation placement, that is not able to absorb electric vehicle infrastructure integration effectively at other nodes or a distributed placement. This means, as soon as the EVCQ is placed at any other node or more distributed within the grid, load problems are bound to occur.

Considering the longevity of distributed power generation, it should be implemented at nodes that can cope with different placements of electric vehicle charging infrastructure. Ideal location for such task are stable nodes located at intersections. Therefore, making the power generation beneficial to multiple branches at once. Otherwise, a need to upgrade

branches back to intersection, for the power generation to have effect in parallel branches could arise. The most stable/least sensitive nodes can be taken from column $\left(\frac{d\Delta U}{d\Delta P}\right)$ in table 4.2. Considering this node order, the first three nodes branching of (R3, R4, R6) are considered for power injection integration during this work.

4.2 Variable Transformer

Variable Transformer can be used to step up or down the voltage. Stepping up the voltage will result in a reduced current. This can lead to a line that was previously overloaded to be within its working limits again. Therefore, no grid expansion or other optimization is needed. Only the voltage at every grid node must still be within the voltage band limits after the voltage increase.
In order to determine the relevance of variable transformer for this work a small preinvestigation is made. Node 14 is chosen out of three most sensitive nodes, that are being investigated during this work. There are a total of 184 households in the grid (see chapter 3.3.2). Considering the minimum penetration of charging infrastructure (scenario A), will result in a total number of approximately 9 EVCU. The amount of charging units to be integrated, is then multiplied with the predefined power (3,7 kWh), for one charging unit (see chapter 3.3.1). This results in a total load of 33,3 kWh connected to node R14.
The integration of the above mentioned load to node R14, will results in the line utilization shown in figure 4.1. The lines L1, L2 and L3 are overloaded. The transformer between node R1 and K0 is operating at 92,3 % of its capacity, and thereby still within it's operating limits.

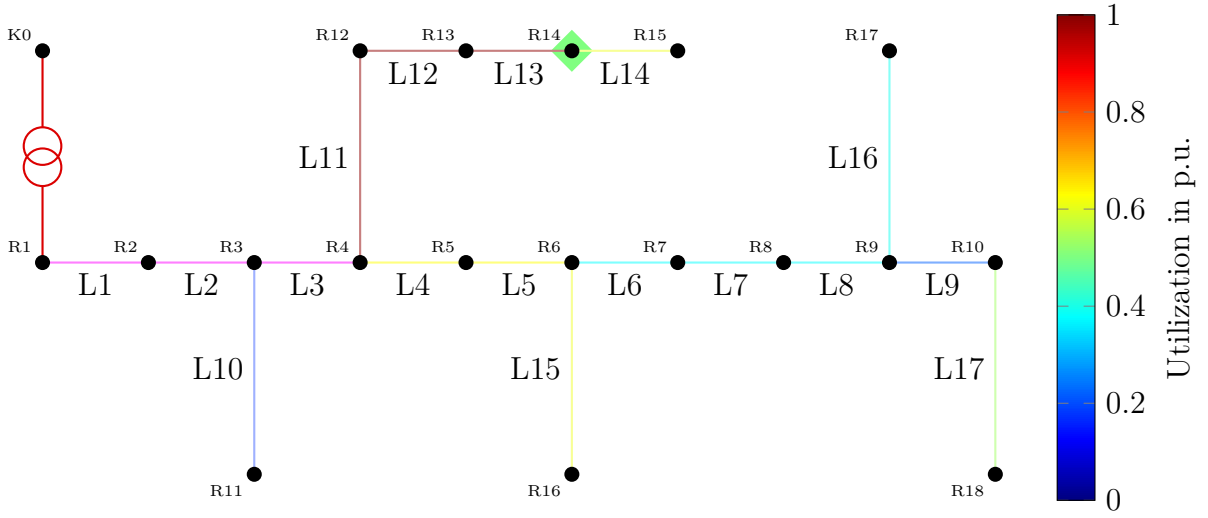

Figure 4.1 Line utilization with nine charging units integrated at node R14

In order to compensate the three overloaded lines, a variable transformer is installed.

Stepping up the voltage to the allowed maximum of +5 %, results in a line utilization seen in figure 4.3. The voltage at each node is still within the −10 % to +5 % voltage margin after stepping up the voltage (see figure 4.2), and thereby adhesives to the voltage band compliance. The limiting factor for a further voltage increase is node R1, which is connected right to the low voltage side of the transformer.

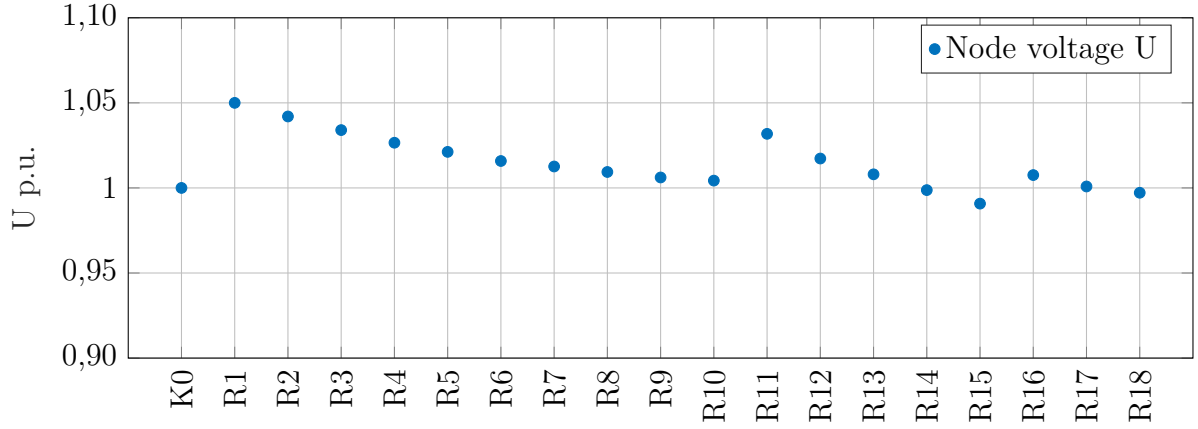

Figure 4.2 Node voltages using a variable transformer to step up the voltage by 5 %

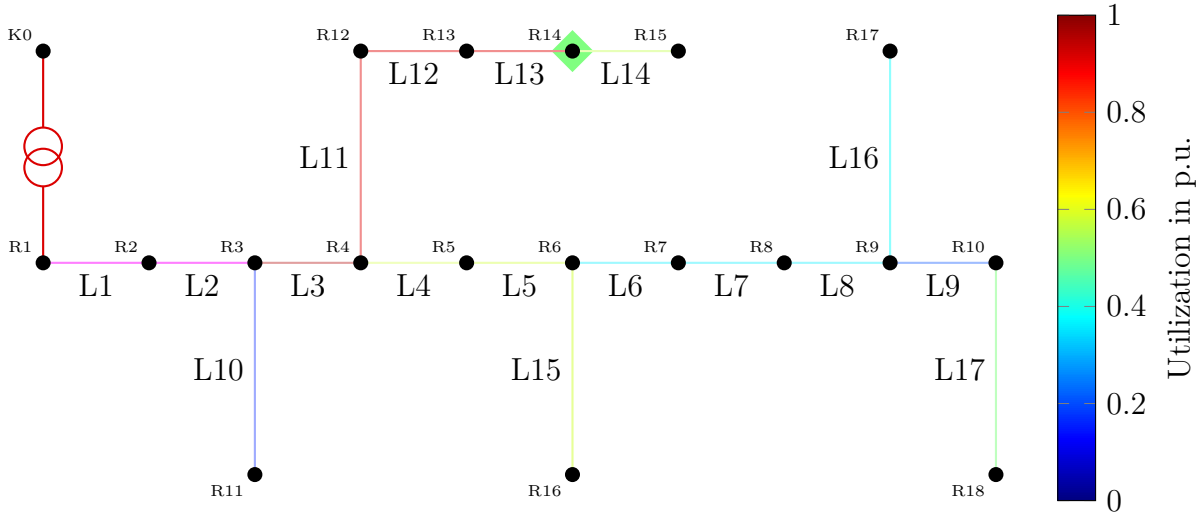

Figure 4.3 Line utilization with nine charging units integrated at node R14 and the voltage being stepped up by 5 %

Comparing figure 4.1 and 4.3 shows, that the line L1 and L2 are still overloaded. Only the line L3 is back within its working parameters, due to the voltage increase. The individual line utilization in relation to their respective current carrying capacity is displayed in table 4.4.

Table 4.4 Line utilization from transformer to node R14 based on current carrying capacity

	utilization	
Lines	regular	stepped up
L1	110,0 %	101,8 %
L2	110,0 %	101,8 %
L3	103,3 %	95,6 %
L11	98,7 %	90,9 %
L12	98,7 %	90,9 %
L13	98,7 %	90,9 %

The average utilization gain by stepping up the voltage is 7,9 % during this preinvestigation. The variable transformer is able to successfully reduce the line utilization for a single cable and bring it back in its working parameters. In the next scenario B, with twice as many EVCU, it is not possible to back any lines back into their working limit by only increasing the voltage. According to [16] the price difference between a regular and variable transformer is approx. 12000 €, in respect to the benchmark network. The cost to reinforce line segment L3 using conventional methods is 5022,50 €. Therefore, variable transformers do not benefit significantly enough to be taken into closer considerations.

4.3 Grid Uncertainties

Generally, network simulation are performed using ideal models. In reality grid variables are subject to fluctuation during the daily operation [31]. There are uncertainties in the power production and consumption. To ensure constant supply of power, the grid operator must have a certain amount of reserve power available at all times [67]. The reserve power is used to overcome unexpected power peak. Furthermore, there are uncertainties regarding the grid parameters. The grids ability to carry power is mainly dependent on the lines temperature. During this section, the influence of temperature uncertainties on the residential subnetwork will be analysed.

Figure 4.4 displays a cables temperature probability density function. The characteristic parameters have been adapted according to the probability density from [36]. This describes the temperature distribution for an overhead line. The temperature data was collected in one hour intervals over the duration of one year. As a consequence of lack of data, the parameters will be applied to underground cables. Feeding the data into equation 2.54 & 2.55 results in a mean value of 35°C and a standard deviation of 10°C.

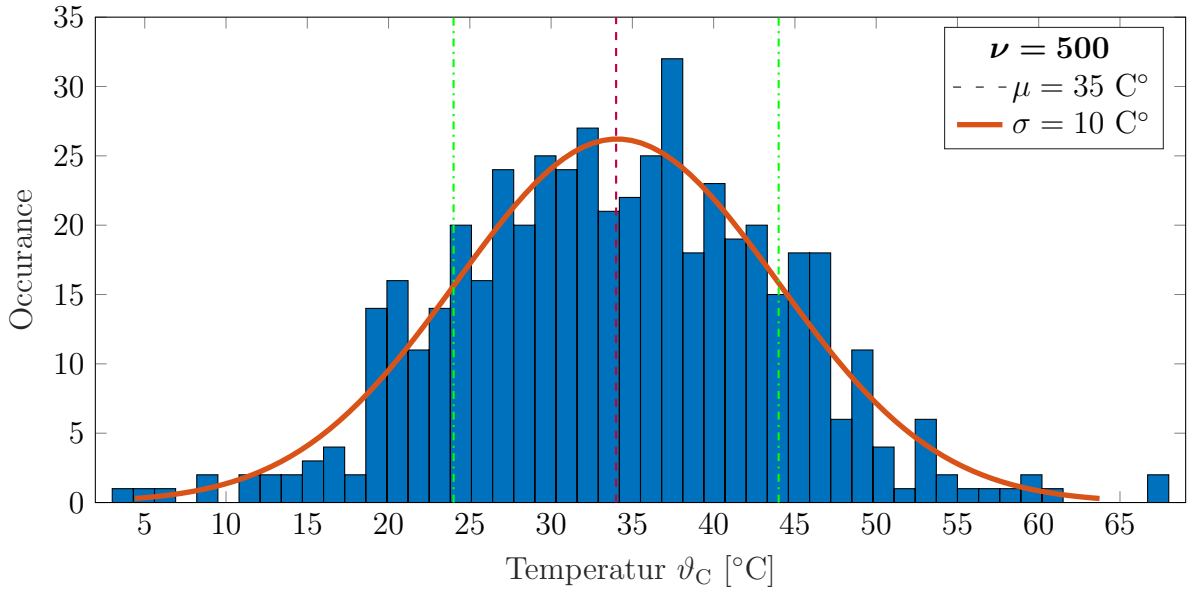

Figure 4.4 Gauss distribution cable temperature distribution

Just as the temperature fluctuates, so do the cable parameters. The temperature coefficient α_0 depends on the conductor material and can be found in standard literature [45][11]. For aluminium the temperature coefficient ranges between $0,00347 - 0,00409$ $^1/_K$ at $\vartheta_0 = 20$ °C. The copper temperature coefficient can be neglect since all cables in the residential sub-network are made from aluminium [53].

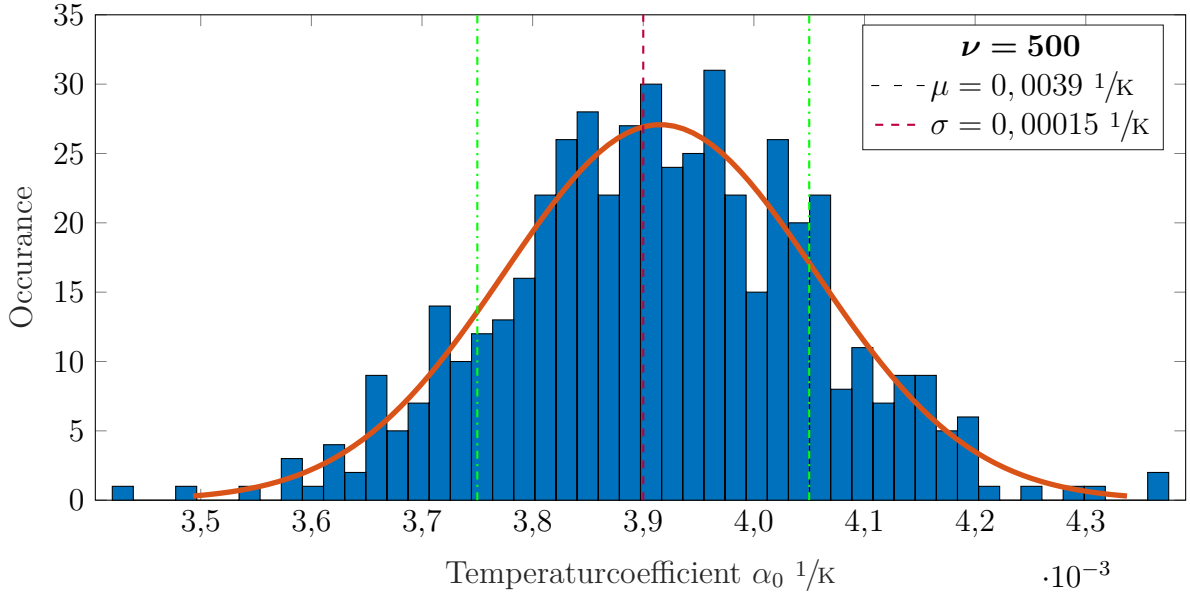

Figure 4.5 Gauss distribution aluminium temperature coefficient distribution

In the distribution network the temperature has a big impact on the loop resistance [30].

Furthermore, it is possible to neglect the insulator capacitance and conductance in distribution network [30]. During this work, only the dependency of the loop resistance R_0 on the temperature ϑ is analysed, since there are only cables in the residential sub-network. The cables resistance R at the current operating temperature ϑ_C is calculated using the following equation [4].

$$R = R_0 \left(1 + \alpha_0 \left(\vartheta_C - \vartheta_0\right)\right) \tag{4.1}$$

Using the Monte Carlo simulation described in section 2.10, the influence of the cable temperature and temperature coefficient onto the loop resistance R is being examined. For each of the two uncertain input parameters one value has been randomly generated for all 500 iteration steps. The distribution of those 500 generated values is displayed in figure 4.4 & 4.5. After each iteration step of the Monte Carlo simulation a power flow calculation is performed. Based on the power flow calculation the nodes voltages and lines utilizations is calculated. The results are displayed in figure 4.6 & 4.7 using the IQR. 50 % of all values are within the blue box, with the dark blue line marking the median. The whiskers (black lines) extend to include 99 % of all values. The red x marks the maximum and minimum outliers.

The variation in node voltages under uncertainties is displayed in figure 4.6. The node voltage variance increases with an increase in distance to the transformer and load. The largest variation can be observed at node R15. The minimum recorded voltage over all iteration at node R15 is approximately 0,9038 V p.u., which is still within the grid operational limits (see section 2.7.1). Nevertheless more than 50 % of values fluctuate no more than 0,004 V p.u..

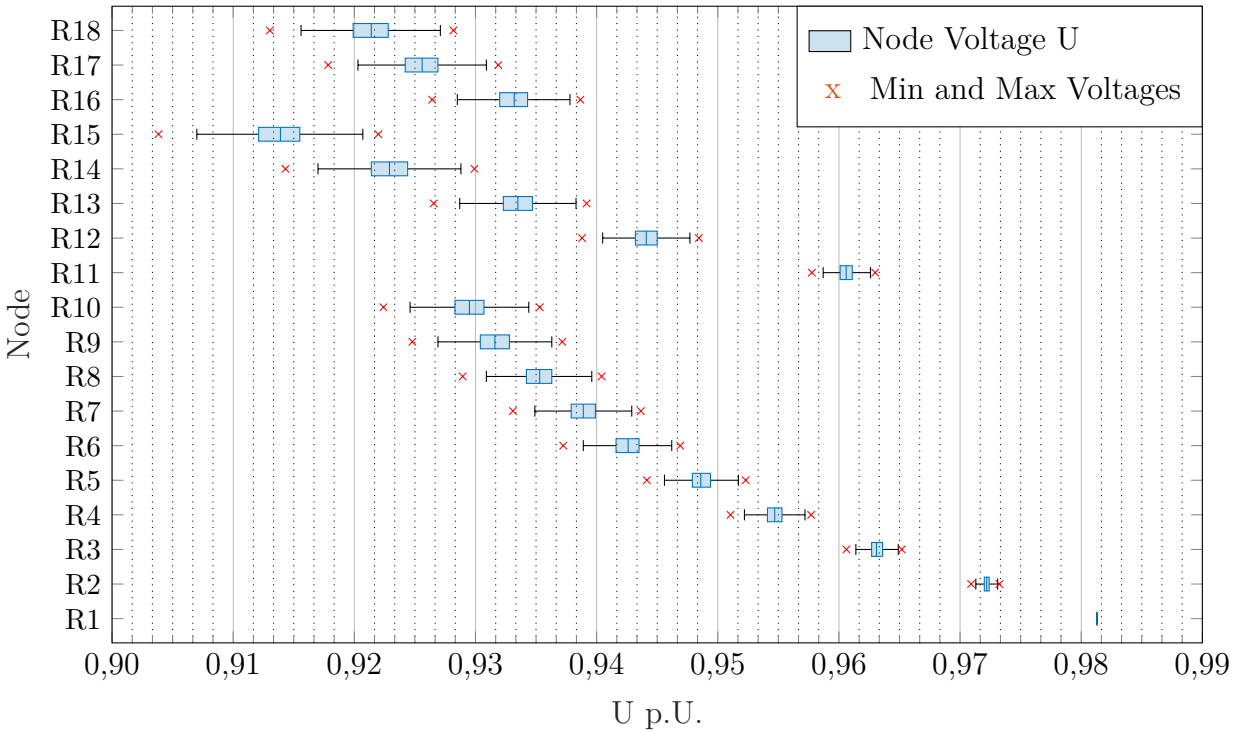

Figure 4.6 Node Voltage variation under cable temperature and temperature coefficient uncertainties

Figure 4.7 displays the line utilization under uncertainties. The graph shows that, neither cable temperature nor temperature coefficient have a significant influence on the line utilization. This can be observed in the close proximity of maxima and minima of each line.

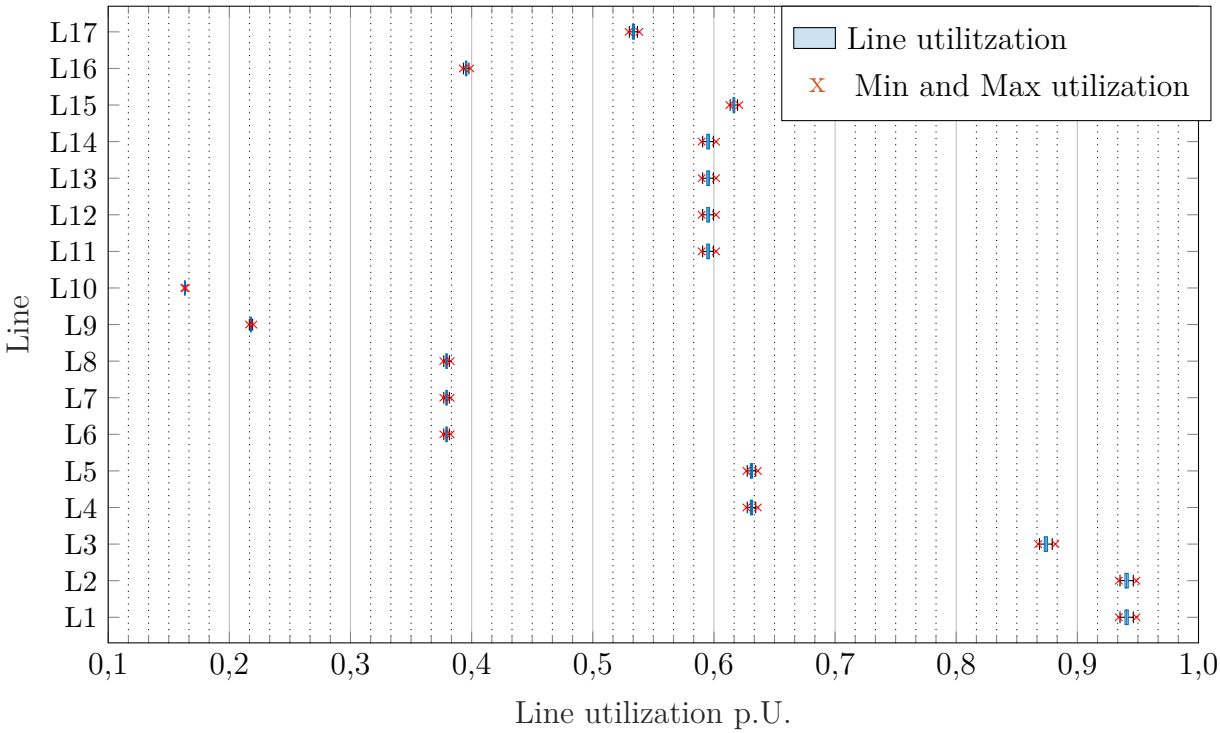

Figure 4.7 Line utilization variation under cable temperature and temperature coefficient uncertainties

Considering the results obtained through the Monte Carlo simulation, the cable temperature and temperature coefficient uncertainties do not seem to greatly influence the grid lines utilization. Figure 4.6 suggests a voltage band violation is more likely to occur, compared to a line utilization violation. Since the residential cigre benchmark grid is of radial nature, with no additional power producers, the node voltage will continue to fall with its distance to the transformer. Therefore the algorithm will be run twice. Once with normal parameters and second time using the temperature and temperature coefficient, which resulted in the minimum voltages seen in figure 4.6.

5 Solution Methodology

The strategic grid reinforcement algorithm provides an insight to the optimal reinforcement of low-voltage networks. Based on predetermined levels of freedom and restrictions mentioned in chapter 3, the algorithm conducts a fundamental grid improvement strategy. The main limiting factors during the planning process, are the selected scenarios with their associated amount of electrical vehicle charging units and the chosen electrical equipment for grid compensation. Within the algorithm the methods for grid compensation will then be optimized regarding the lowest total cost. During this, numerous different combination will be evaluated and marked regarding their sustainability. The scenario and node selection limits the degree of freedom and makes the amount of possible options to analyse and solutions finite, which are the general characteristics of an optimization problem [17]. Such types of problems require a high amount of computing power [17], and can in general be solved mathematically.

Precise calculation methods are solving the problem in an finite amount of steps. The calculation power needed for such task increases with every additional grid node or compensation method. The restraint to only the three most and least sensitive nodes and designing three scenarios limits the growth of the problem; thereby, applying heuristic to the solving approach. Heuristic methods are based on hypothesis, analogies or experience, therefore it is harder determine the quality of results. This lack validation illustrated the draw back of applying such methods. In addition stochastic optimization was used to account for gird uncertainties regarding the lines temperature and temperature coefficient (see chapter 4.3). Analysing the full grid would take a lot of computing time, which would only continue to grow exponential with additional variables. For this reason, a case study was done using the cigre benchmark grid, to limit the possible options (see chapter 3). Therefore only the most import nodes and parameters are accounted for in the algorithm. This results in the reinforcement algorithms being a combination of exhaustive search and reduction of complexity.

5.1 Basic Concept

The algorithm can roughly be divided in the three sections initialization, grid reinforcement and cost calculations. In the first section additional loads get integrated into the grid based on the scenarios in section 3.3.3. Each of the three scenarios A, B & C has a different number of households, which results in changing amounts of EVCUs. Following the additional load, all power flows within the network are calculated. This is done to determine the equipment utilization and check for grid compliance violations. Should there be a compliance issue, the grid reinforcement section of the algorithm starts. Based

on the previously performed power flow calculation results, the possible grid reinforcement options are worked out. The algorithm also includes the option to constrain certain grid reinforcement methods. Restrictions can be adjusted to fit geographical locations. During this work no restrictions regarding reinforcement methods for certain line sections have been made (see chapter 3). In the final step the cost for each grid reinforcement option is calculated. The cost for the the different grid reinforcement options is based on section 3.4. The cheapest cost of different reinforcement possibilities is then displayed, together with their respective needs for grid reinforcement. The fundamental procedure of the algorithm is displayed in figure 5.1, with a detailed explanation of each algorithm section following.

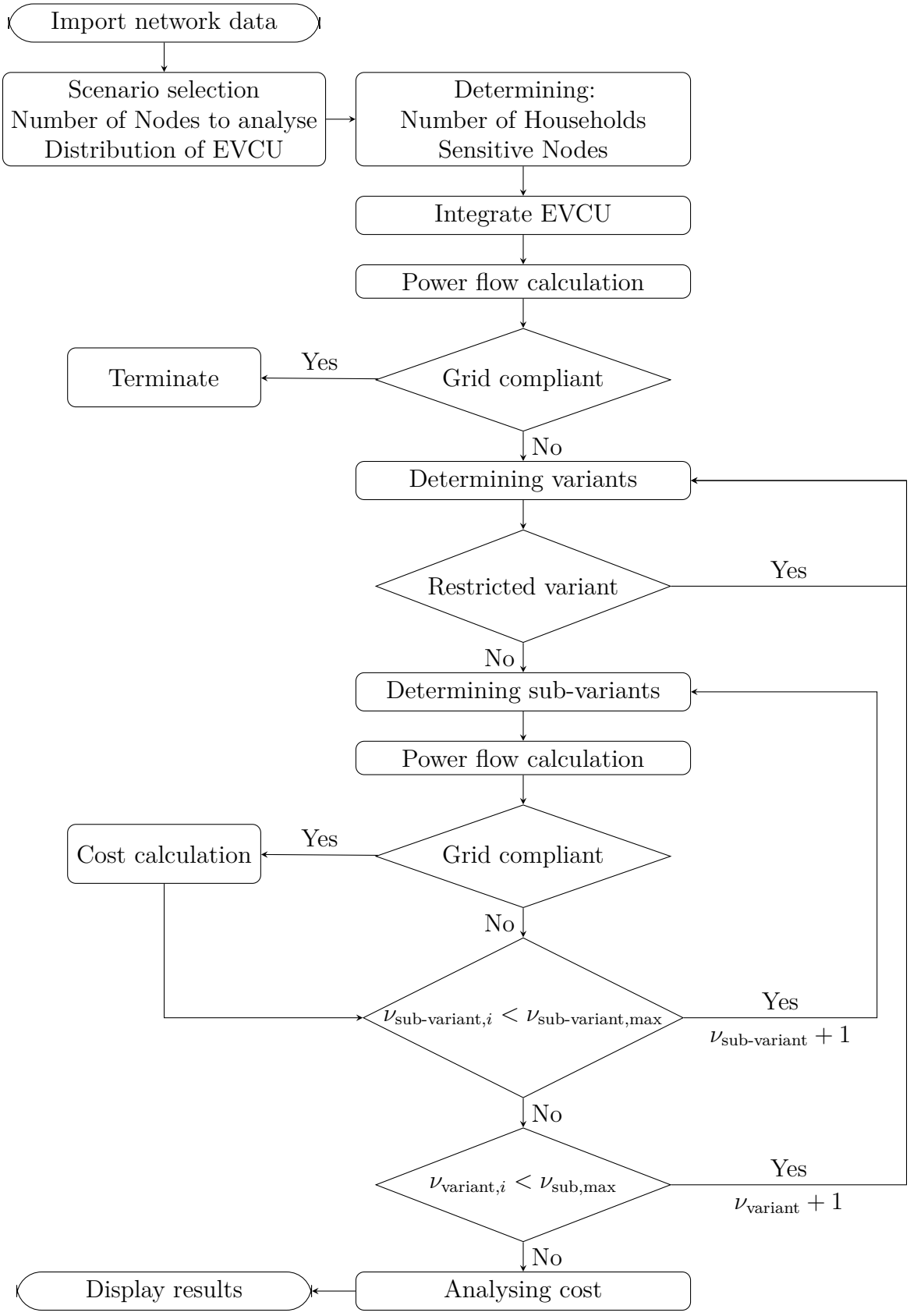

Figure 5.1 Flowchart grid reinforcement algorithm

5.2 Initialisation

Within the grid reinforcement algorithm, the scenarios, number of grid nodes to be analysed for placement of EVCUs, and their distribution are variables. These variables need to be selected at the start. The number of grid nodes taken into account for the placement of EVCUs greatly effects the required computational effort, since every additional node increases the number of possibilities exponentially.
The scenario variable specifies the penetration of charging infrastructure. Based on the number of households, that has previously been determined (see section 3.3.2) and the chosen percentage of penetration, the total quantity of EVCUs will be identified. The charging units are then converted to active power loads as described in section 3.3.1. The sensitivity of all nodes respective to each other is determined using the sensitivity matrix (section 2.8). This results in the sensitive order displayed in section 4.1, for the cigre benchmark network. Based on this order, the amount of nodes to be analysed are selected, starting from most to the least sensitive.
The calculated load, that is to be integrated, is placed at the selected nodes via two options. The total load amount can either be placed concentrated or distributed. With a concentrated implementation the entire load is placed at a single node. Meaning that the following steps need to be repeated for every selected node. Using a distributed placement, the load is equally distributed and placed over all selected nodes.

5.3 Grid Reinforcement

Following the initialisation phase and the load integration from EVCUs a power flow calculation is performed. This is done to determine the cables current-carrying and voltage band compliance (see chapters 2.7.1 & 2.7.2). Should any of those two restrictions be violated the grid reinforcement process starts and tries to find the best possible solution to bring the grid back to a state of normal operation. For better understanding, the process is demonstrated on the example grid in figure 5.2. In the example grid a load has been integrated at node R5, resulting in Line L2 and L4 being over utilized. The transformer and other lines are not considered during the demonstration.

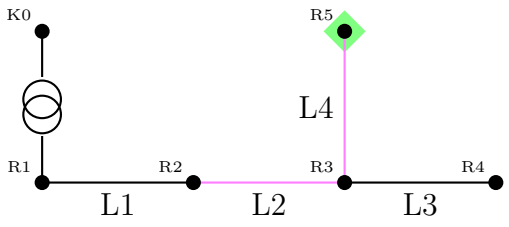

Figure 5.2 Small residential example grid

After identifying the over utilised lines the various equipment combinations are established. The algorithm has the possible variation options: A.) single cable, B.) multiple cables or C.) power injection using Lithium-ion storage or CHP. While cables are placed between nodes, DER is placed at the node itself. The nodes for placement of power injection is based on based on the sensitivity matrix as well (see chapter 4.1). When DER is placed inside the grid all node connections, that are not directly in line from the power injection node to the EVCQ nodes, are not considered for grid expansion. This results in the following variants matrix. Setting grid restrictions would eliminated the impossible grid variant options, there reducing the total number of calculations. If gird restrictions are set, the impossible variant options

Table 5.1 Variant options for small residential example grid

Variant	L2	R3	L4
1	A	-	A
2	A	-	B
3	B	-	A
4	B	-	B
5	-	C	A
6	-	C	B

Each variant option has multiple sub-variants. The cables have different sizes, that can be used and the DER has different power injection levels. These sub-variants can again be combined among each other. The cable sub-options are restricted by their current-carrying capacity. The new cables current-carrying capacity, or the sum if multiple cables have been laid, must be greater than the previously installed capacity. Furthermore, the minimum implemented DER power must equal or greater, than the combined power requirements of the grid and EVCUs minus the current maximum possible network power. The sub-variant matrix for variant 3 from table 5.1 using only the first two cable options from table 8.7 is displayed the following.

Table 5.2 Sub-variant options for variant 3 of the small residential example grid

Sub-variant	L1 Variant B	R3	L4 Variant A
1	UG3x1	-	UG1
2	UG3x2	-	UG1
3	UG3x3	-	UG1
4	UG3x1	-	UG3
5	UG3x2	-	UG3
6	UG3x3	-	UG3

For every sub-variant option of all variants, a power flow calculation is performed to determine the grid compliance. Should the power flow calculation not converge, or result

in a grid compliance issue, the corresponding sub-variant will be marked as not suitable. The cost calculation will be skipped for this sub-variant and the algorithm continues.

5.4 Cost Calculations

When a sub-variant adheres to all compliance restrictions the cost will be calculated. The cost calculation depend on the variant and previously defined grid restrictions, which are dependent on the geographical grid conditions. During the cost calculation the price for each suitable sub-variants is determined and saved in an independent matrix, which list the price for each sub-variant. Within this matrix the cost for transformer, cable and DER are separately listed, thereby allowing for more detailed comparison of specific cases and major cost factors if necessary. The DER cost is calculated twice, once for lithium-ion storage and once for CHP. The specific price structure that is used can be found in section 3.4. Considering the sub-variant displayed in 5.2, a node distance of 30 m and no conduits, results in the following cost table. Since the transformer is not over utilized and Lithium-ion or CHP has not been used in the above mentioned sub-variant, their respective columns are empty.

Table 5.3 Cost of sub-variant options for variant 3 of the small residential example grid

Sub-variant	Transformer	Cable	Lithium	CHP
1	-	10 548,53	-	-
2	-	15 593,98	-	-
3	-	20 639,43	-	-
4	-	10 090,90	-	-
5	-	15 136,35	-	-
6	-	20 181,80	-	-

Up on calculating all prices, the final cost is being analysed. For this, the prices of each sub-variant is summed up. The lowest total of each sub-variant is then determined and used to represent the variant cost. The different variant cost are then compared to each other, in order to find the cheapest possible grid reinforcement option.

6 Discussions

This chapter examines the economical cost for grid expansion dependent on the penetration of electric vehicle charging equipment. The three scenarios A.) 5 %, B.) 10 % and C.) 20 % correspond to an integration of 9, 18 and 36 EVCUs into the grid. The cost calculation are based on the prices in section 3.4. Feeding the grid reinforcement algorithm with these prices, resulted in the cost displayed in this chapter. The different scenarios are evaluated in regards to the following variables:

- Node sensitivity
- Distribution of electric vehicle charging equipment
- Energy storage vs conventional grid expansion

To give a deeper insight into the cost structure, the price for the transformer, conventional grid expansion and energy storage units are displayed separately. Dependent on geographical conditions, the cost might increase or decrease. Therefore, when transferring the conventional grid reinforcement cost, the general division between surfaces (see section 3.4) must be adjusted to fit the circumstances. All prices displayed throughout this chapter are applicable to urban areas.

The graphs throughout this chapter display the grid reinforcement cost when implementing the loads, that are resulting from the integration of EVCUs, at the nodes shown in the legend. The whisker lines in each plot gives the maximum cost outcome when accounting for uncertainties. Furthermore, the baseline set in chapter 3.1 is valid for every analysed case. This base utilization has to be taken into account when extrapolating the results to other grids.

Since the cigre benchmark network has no restriction regarding the cable options, the multiple cable approach is always the most cost effective approach. This results from the cigre residential sub-network not having any existing conduits, nor space restrictions. In addition, the reduction of the current carrying capacity through multiple lines, only has notable impact when higher numbers of cables are placed in one trench/conduit (see section 2.7.2). Not accounting for uncertainties, the algorithm places a maximum of three parallel cables in any given scenario in cigre benchmark network.

6.1 Node sensitivity influence

In this section, a closer examination on the influence of the node sensitivity on the total cost. For this evaluation, the three most and least sensitive nodes (see section 4.1) are first

analyzed separately for each scenario. The average cost of each scenario is then compared regarding its sensitivity.

6.1.1 Most Sensitive Nodes

The influence of the node sensitivity on the grid expansion cost is first analysed. For this analysis, the EVCUs are all integrated at the same grid node. Figure 6.1 shows the cost to upgrade the grid in order to compensate the additional loads from the different amount of charging units, that are being integrated at either node R14, R18 or R15.

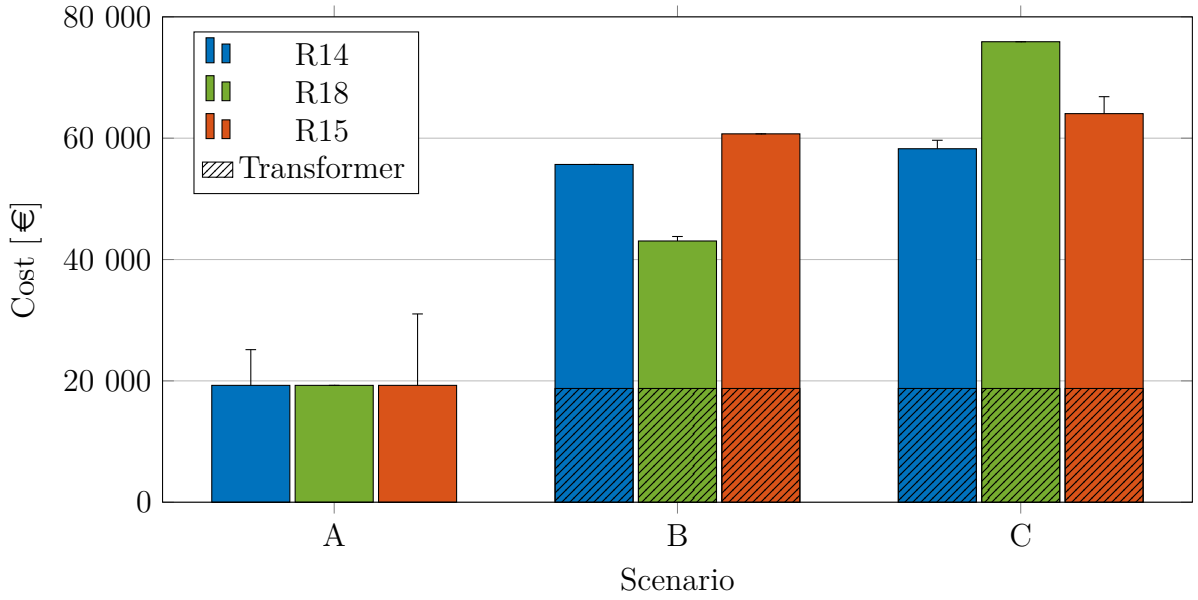

Figure 6.1 Cost to upgrade the gird for scenario A, B & C at the most sensitive nodes

In the scenario A, displayed in Figure 6.1, the cost stays the same across all nodes. This is due to only the first three lines (L1 & L2 & L3) being overloaded and requiring to be reinforced. The cost increase through uncertainties for node R14 and R15 result from a voltage band violation. The cost increase is a lot higher compared to the other two scenarios, due to additional lines/trenches needing to be excavated. In the other scenarios, the voltage band violations can be compensated through laying more cables in already excavated trenches. As seen in a later cost breakdown (section 6.4), the majority of the cost originates from excavating new trenches.
The following two scenarios B % C, have a further cost increase not only due to greater amount of overloaded lines, but also due to the transformer needing to be upgraded. Since a single upgrade in transformer size is able to handle the load increase for the second and third scenario, the transformer cost stays constant. Furthermore, when comparing the grid upgrade cost to node R14 and R15 for the second and third scenario, only a minor increase

can be noticed. To be precise, the cost increase is 2591,59 € for node R14 and 3332,04 € for node R15. This slight price increase occurs due to additional cables needing to be layed and work that is connected to this task. The total grid reinforcement cost to node R18 increases with each scenario, due to more lines being overloaded and needing to be reinforced.

6.1.2 Least Sensitive Nodes

The three least sensitive nodes and their cost to upgrade the grid infrastructure up to this point is displayed in Figure 6.2. As with the most sensitive nodes, the EVCU are all placed at a single node throughout each scenario. There are no additional costs related to laying more cables when placing charging infrastructure at node R1, since everything is directly connected to the transformer. Therefore, only the transformer needs to be upgraded for node R1 in the second and third scenario.
Between node R2 and R3 is a cost difference of 6420,26 €, due to the one extra line (L2) being overloaded. Except for this price difference, the conventional grid reinforcement cost for node R2 and R3 stays constant throughout all three scenarios, when excluding the transformer cost. As with the most sensitive nodes, the transformer only needs to be upgraded for scenario B and C.

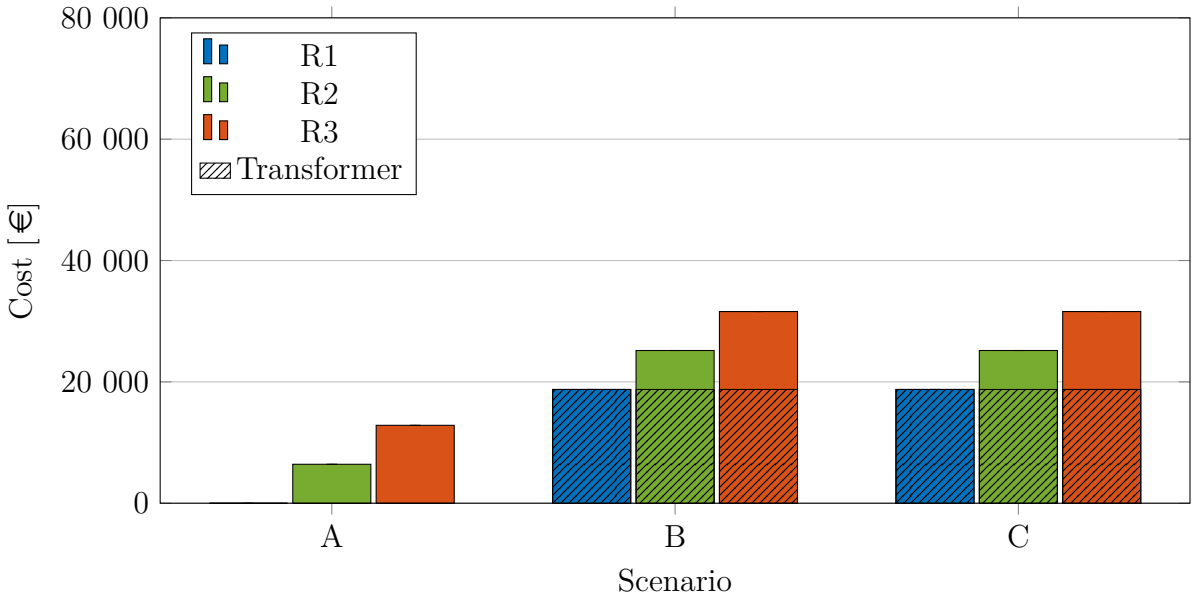

Figure 6.2 Cost to upgrade the gird for scenario A, B & C at the least sensitive nodes

6.1.3 Least & Most Sensitive Nodes Comparison

Figure 6.3 displays a cost comparison between the three most and least sensitive nodes. For this comparison, the total cost of R1, R2, R3 and R14, R18, R15 has been averaged.

The cost for the least sensitive nodes only increases from scenario one to two, while the cost for the most sensitive nodes rises with each scenario. The cost increase for the most sensitive nodes is due to the additional lines needing to be upgraded. The transformer cost is the same between a distributed and concentrated EVCU integration. Furthermore, the average grid reinforcement cost for the most sensitive nodes increases by the factor 3,5 when doubling the amount of EVCU in scenario B, but only 4,2 when quadruplicating the amount of EVCU in scenario C.

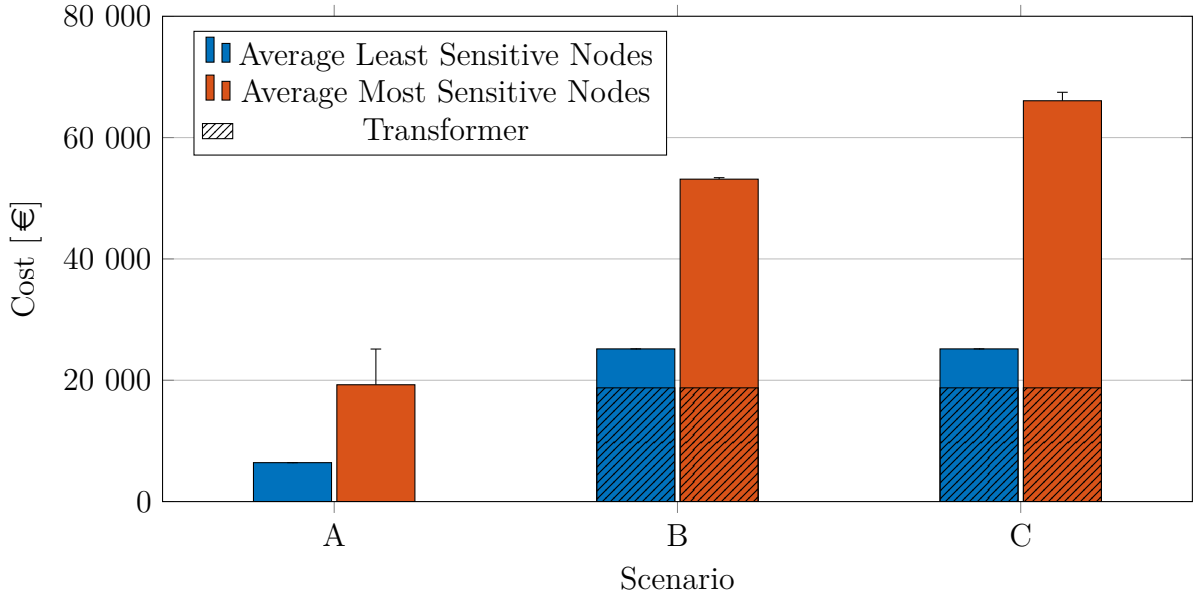

Figure 6.3 Comparison between the average cost of the most sensitive nodes (R14,R18,R15) and the least sensitive nodes (R1,R2,R3)

6.2 Distributed Power

Instead of only upgrading the grid infrastructure through line and transformer upgrades, it is also possible to place lithium-ion storage units or CHP within the grid, thereby avoiding part of the conventional grid reinforcement cost of placing new cables.

6.2.1 Lithium-Ion Storage

Figure 6.4 displays the total grid reinforcement cost when integrating lithium-ion storage at the best possible node. For nodes R14 and R15, the lithium-ion storage was integrated at node R4, while for node R18, it was integrated further away from the slack node at node R6. This leads to an average reduction in line upgrade cost of 19261 € for node R18 and 32101 € for nodes R14 & R15, compared to the conventional approach displayed figure 6.1. Although conventional grid reinforcement methods can be avoided inertly in scenario A, the cost is more than ten times higher when lithium-ion storage is used. In scenario

B and C, part of the grid still has to be upgraded by laying new cables. Comparing the cost of the storage unit in scenario B and C to the line upgrade cost, it can seen that the major cost factor is the lithium-ion storage, which is more than 95 % of the total cost. This shows that even with future price predictions for lithium-ion storage systems, it is not feasible to overcome overloaded grid problems using them. The cost of the lithium-ion storage units needs to decrease by at least a factor of 10, to approx. 35 €/kWh, in order to make them competitive with conventional grid expansions methods.

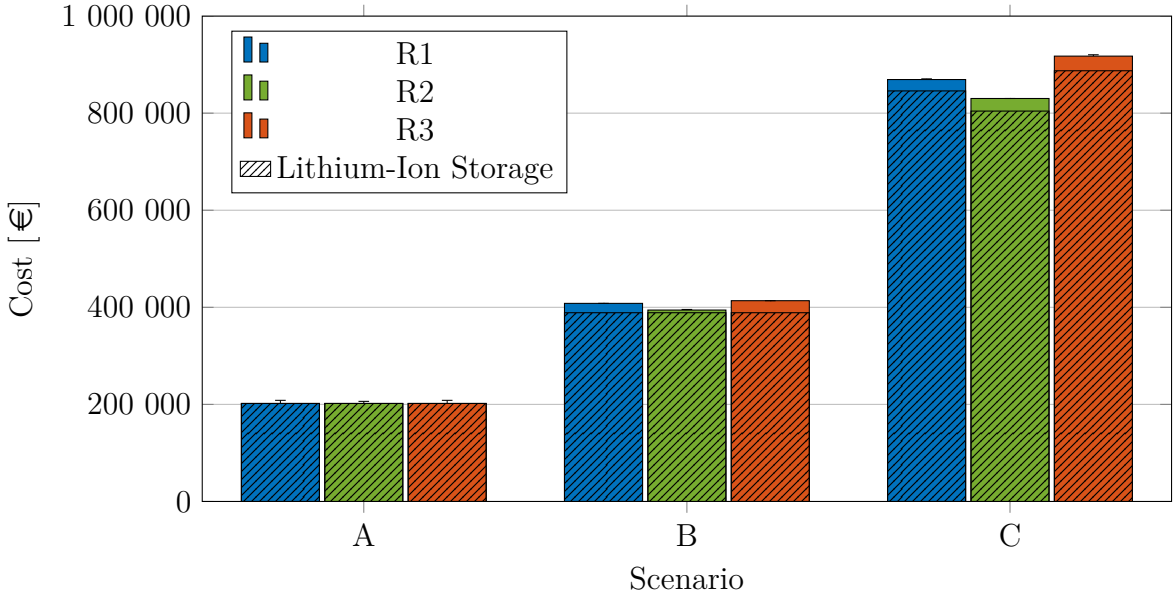

Figure 6.4 Cost to upgrade the gird for scenario A, B & C at the most sensitive nodes using lithium-ion storage

6.2.2 Combined heat and Power

Instead of using lithium-ion storage to reinforce the grid, it is also possible to use CHP. The cost is displayed in figure 6.5. Using CHP, the same conventional grid reinforcement cost can be saved as with the lithium-ion storage. Compared to the other two reinforcement methods, CHP is on average approximately 5,7 times more expensive than conventional grid reinforcement and is close to being half the price of lithium-iron storage. Despite the extra money that can be made, through putting the extant heat to good use not being accounted for. This could potentially increase the benefit of CHP.

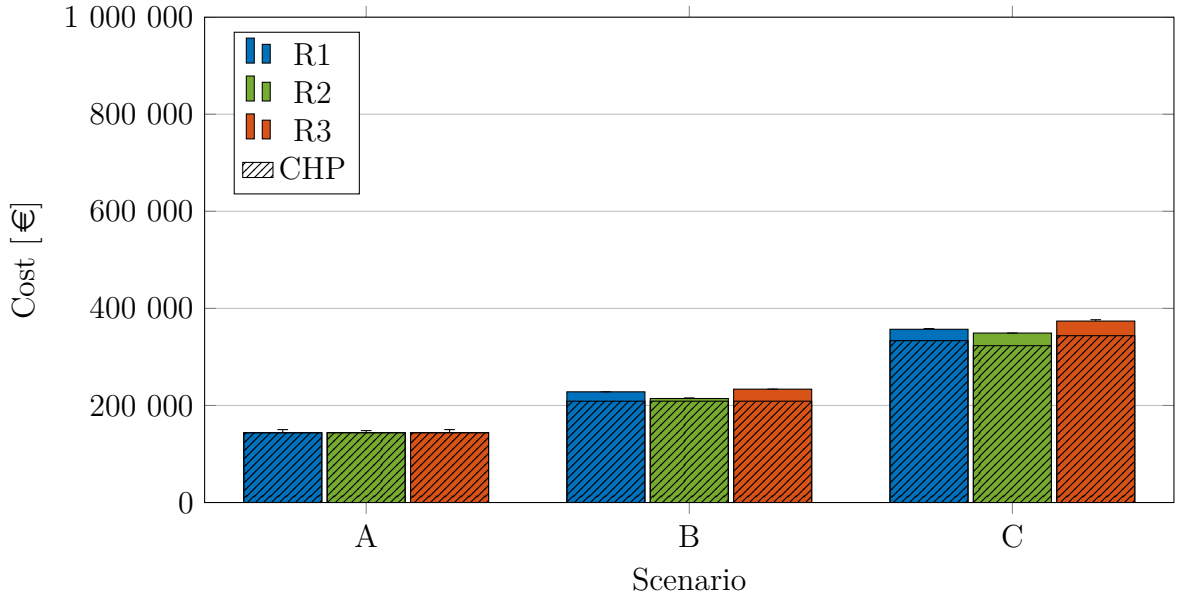

Figure 6.5 Cost to upgrade the gird for different scenarios at the most sensitive nodes using CHP

6.3 Electric Vehicle Charging Units placement

A cost comparison between a concentrated EVCU integration at the most sensitive node R15 compared to an equally distributed implementation over the three most sensitive nodes R14, R18, R15 reveals, that there are only minimal cost differences (see figure 6.6). The grid reinforcement cost in the first scenario is the same, while in the other two scenarios, minor deviations can be noticed. The cost difference between a distributed and concentrated approach is only 8 % in scenario two and 3 % in scenario three. Therefore, it is possible to only evaluated a concentrate implementation of EVCU at the most sensitive node and still be able to fairly accurately predict the total cost of grid reinforcement for a distributed implementation.

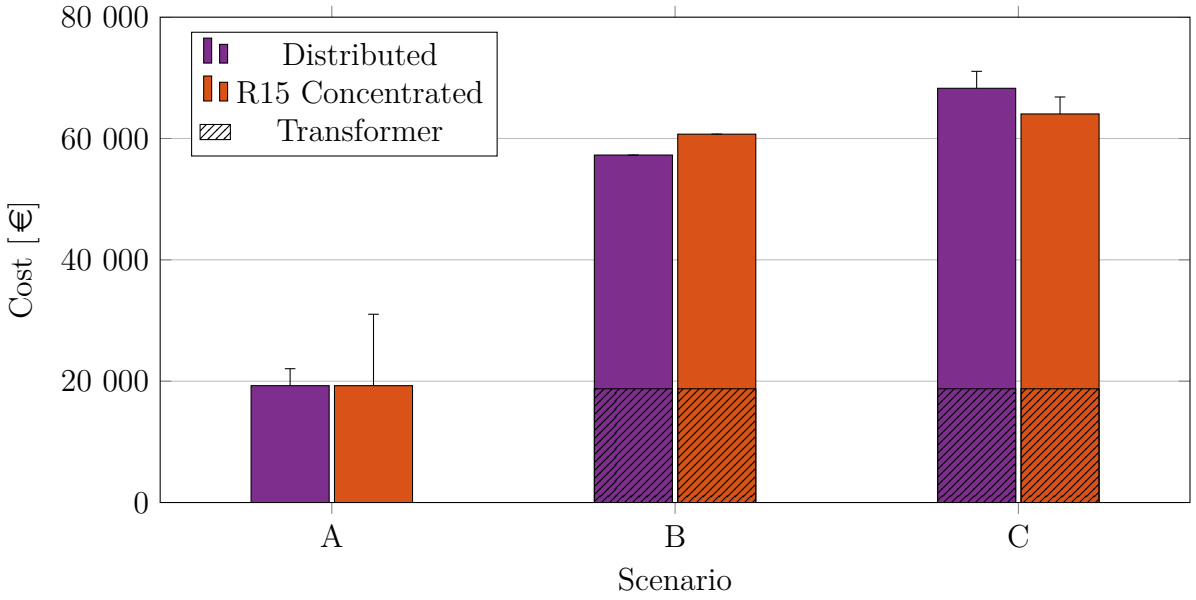

Figure 6.6 Difference in grid upgrade cost using conventional grid reinforcement for concentrated (R15) and distributed (R15,R18,R14) charging infrastructure integration for scenario A, B & C

Figure 6.6 displays the cost for grid expansion using lithium-ion storage for distributed and concentrated EVCU integration. For the concentrated approach, all the EVCUs have been implemented at node R15 and for the distributed approach, the EVCU have been equally distributed over the nodes R14, R18 and R15. During the distributed approach the lithium iron storage unit was placed at node R4 instead of R6, since line segments L4 and L5 would otherwise require to be reinforced. The cost difference between a distributed and concentrated placement is the greatest in scenario C with only 4 %.
Using CHP as grid reinforcement instead of lithium-ion storage (see figure 6.8) results in a maximum cost difference of about 3 % between concentrated and distributed placement in scenario C.

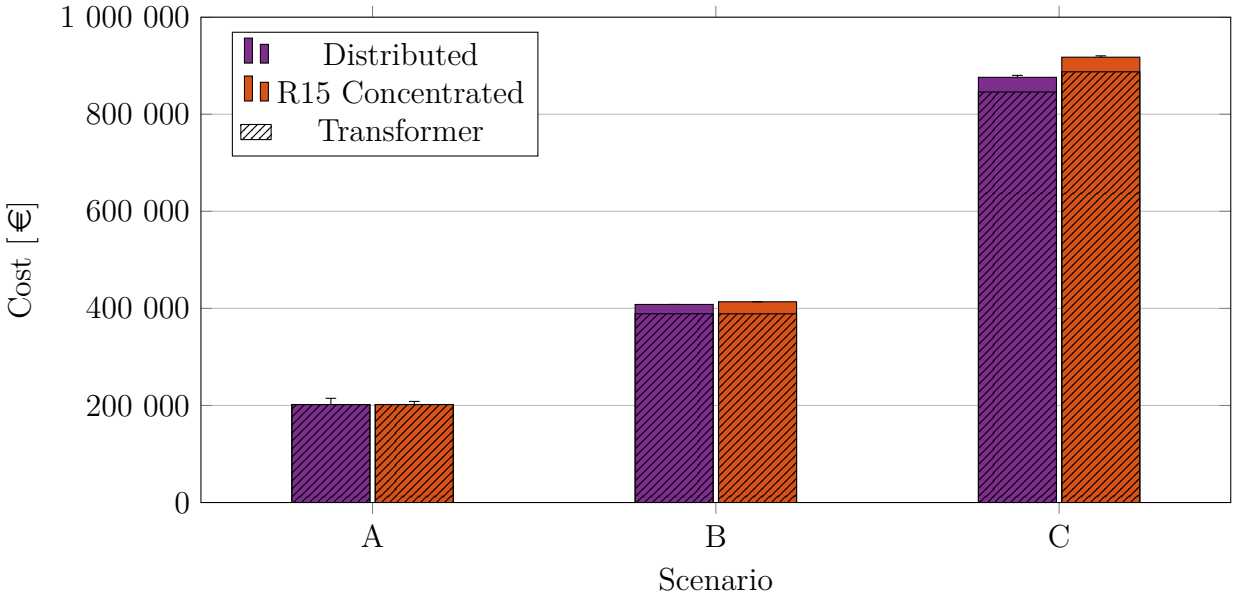

Figure 6.7 Difference in grid upgrade cost using lithium-ion storage at node R4 for concentrated (R15) and distributed (R15,R18,R14) charging infrastructure integration for scenario A, B & C

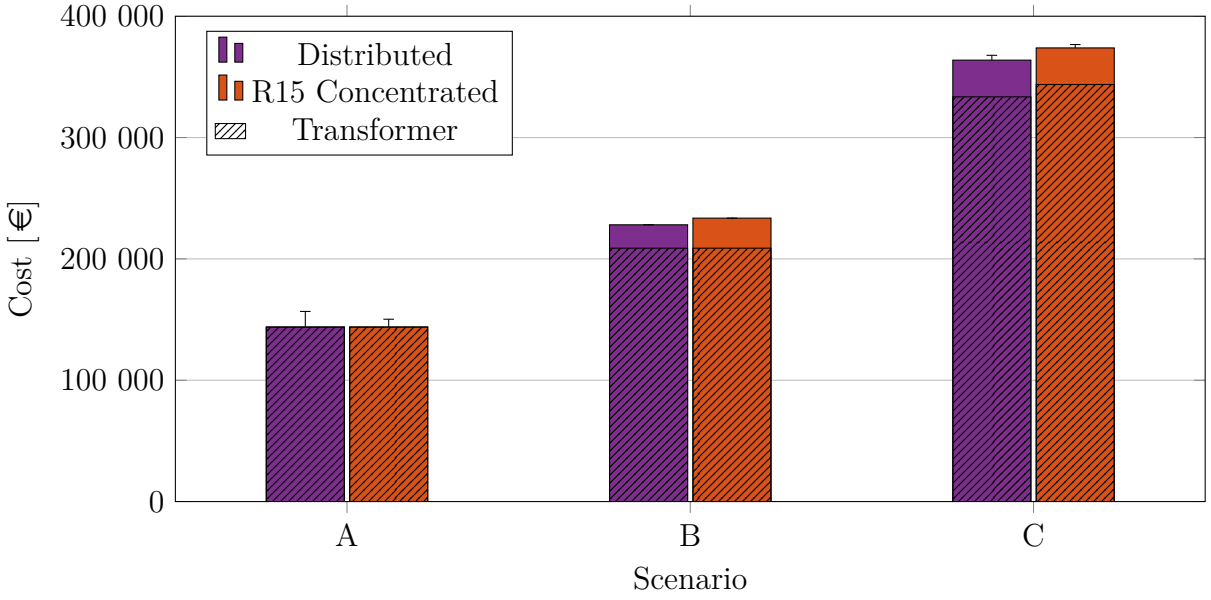

Figure 6.8 Difference in grid upgrade cost using CHP storage at node R4 for concentrated (R15) and distributed (R15,R18,R14) charging infrastructure integration for scenario A, B & C

The results from figure 6.7 using conventional grid reinforcement methods align well with the results from lithium-ion storage (fig. 6.7) and CHP (fig. 6.8). Independent of the chosen grid upgrade method, the cost for a concentrated EVCU integration are almost the same as using a distributed placement. Therefore, it is possible to only consider the most

sensitive nodes within a grid and to use a concentrated load placement to approximate the cost for distributed load integration.

6.4 Cost Allocation

The cost allocation aims to give a brief overview of the cost division. For this analysis, the average cost for all grid reinforcement options regarding node R15 has been calculated. Figure 6.9 displays the cost breakdown for conventional grid reinforcement. The equipment cost being the lowest part only makes up 2,8 % of the cost, while the labor cost makes up almost 55 %. The labor cost is also the biggest fluctuating factor when taking into account other countries [42]. The cable cost is connected to the international copper price and is therefore nearly the same everywhere. The transformer and associated equipment are linked again to the labor cost of the country that they are produced/build in.

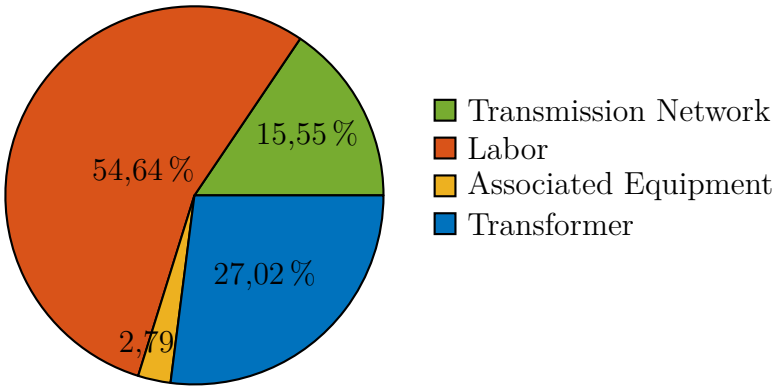

Figure 6.9 Cost division for conventional grid reinforcement

Figure 6.10 & 6.11 display the cost allocation for lithium-ion storage and CHP respectively. The overall cost of using lithium-ion storage as grid reinforcement is more than two times more expensive in comparison to CHP. Therefore, the cost for the building and conventional grid reinforcement is about half times as much in comparison two using CHP for grid reinforcement. The biggest difference between the to options is the operational cost. Using the lithium-ion, the operational cost accounts for about 19 %, while it is only 3 % for CHP. Therefore, lithium-ion storage units could increase their visibility by decreasing the operational cost, thereby leaving more freedom for the manufacturing cost.

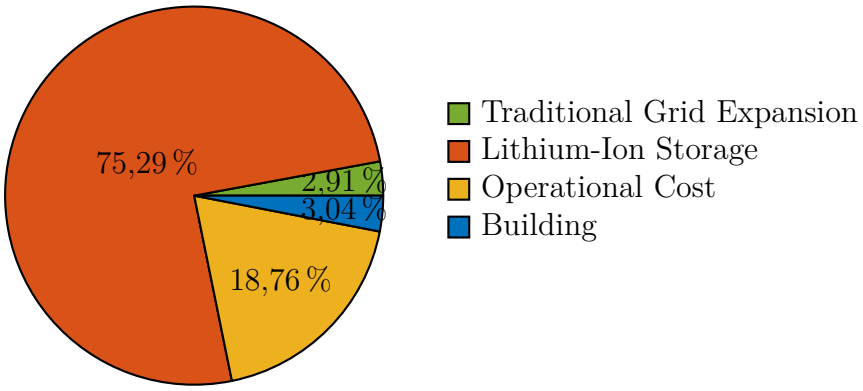

Figure 6.10 Cost division for grid reinforcement using lihtium-ion storage

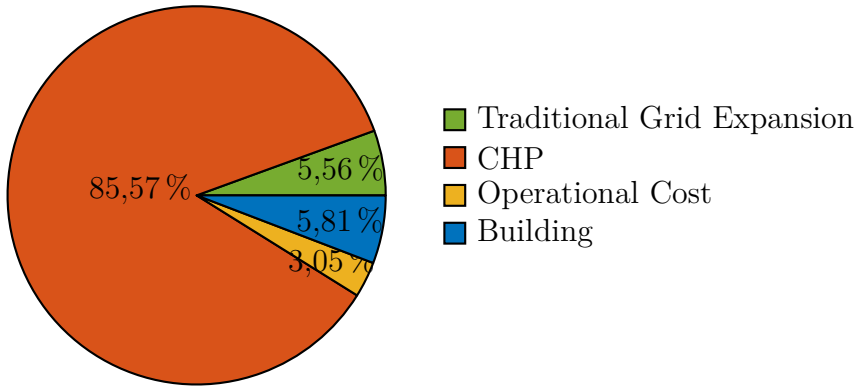

Figure 6.11 Cost division for grid reinforcement using CHP

7 Summary and Conclusion

This work investigated the cost effective reinforcement of LV networks that have been overloaded due to the integration of EVCQ using a grid reinforcement algorithm. For this investigation, a benchmark network was utilized on which basic assumptions regarding the electric vehicle charging number and power were made. Furthermore, the costs for different grid reinforcement options in urban areas was established. Novel methods using conventional grid reinforcement, variable transformers, lithium-ion storage and CHP were considered. In addition, uncertainties through cable temperature and temperature coefficient were depicted and evaluated.

In chapter 3, the framework for the analysed case is established. As a suitable grid, the cigre benchmark LV residential sub-network was selected, since literature research revealed, that a majority of electric vehicle charging is done at home. Additionally, the approximate number of households within the benchmark model was derived using the simultaneity factor for different degrees of household electrification. This examination revealed that approximately 184 dwellings are located within the residential sub-network. In order to overcome the uncertainties regarding the quantity of electric vehicles within the grid, estimations using current vehicle statistics and future set goals by government were made. Through these estimations, three scenarios using different electric vehicle penetration depths have been developed. In scenario A, 5 % of all household in the grid were found to have an electric vehicle, in scenario B, 10 % and in scenario C, 20 %. Furthermore, the definition of "charging unit" was introduced to resolve the numerous different EVCQ active power ratings. One charging unit was defined to equal 3,7 kW. The residential sub-network was constructed in MATLAB to examine the initial grid state, which revealed that all node voltages were compliant with current grid codes and no lines were over-utilized. The initial line utilization for the whole residential sub-network is 55,49 % and the transformer utilization is 84,64 %. For resolving grid congestions, conventional grid reinforcement, lithium-storage systems and CHP were selected as grid reinforcement methods. The three methods and their prices were modelled. Since available literature suggests further breakthroughs in lithium-ion batteries for the upcoming years are to be expected, price projections for the year 2025 were used during the cost analysis, while the current CHP prices were used, since no major future price reductions are expected. The price split for the conventional grid reinforcement approach is composed of official industry reports and internal industry documents.

Chapter 4 conducted a preinvestigation into the case outlined above to determine the influence of node sensitivities, variable transformers, cable temperature & temperature coefficient uncertainties. The gird node's sensitives were used to provide insight into the effect of EVCQ integration on the grid and its nodes. The nodes sensitivity was determined

using the load torque approach and the sensitivity matrices, with both methods resulting in approximately the same node sensitivity ranking. Based on this ranking, the nodes for the integration of EVCU were selected. Furthermore, an investigation into variable transformers concluded that the additional load of EVCU could not be compensated using such equipment. This was due to the additional load increase within the grid being too steep. An additional investigation of possible line uncertainties using the Monte-Carlo method revealed that the cable temperature and aluminum temperature coefficient have some effect on the residential sub-network. The influence on the line utilization was less than 1 % and therefore not influential enough, while the node voltage had considerable fluctuation, which can lead to voltage band violations. To account for these uncertainties, an additional simulation was performed using the highest temperature and temperature coefficient.

Based on the findings in chapter 3 & 4 an algorithm was used to find the most cost-effective grid reinforcement variant for each scenario. The grid algorithm compared each possible grid reinforcement variant and combination to each other. By investigating the three most and least sensitive grid nodes, the maximum and minimum grid reinforcement costs based on EVCU integration could be found. Within each scenario, the cost for the most sensitive nodes only showed a maximum deviation of 12 % to the average, with the line upgrade cost being greater than the transformer cost. The cost difference resulting from uncertainties is at its maximum 4 % greater for scenario B and C. In scenario A, a maximum cost difference through uncertainties of up to 61 % could be observed.
Taking advantage of lithium-ion storage to reduce line upgrade costs at the most sensitive nodes, revealed a reduction of the line upgrade cost by almost half for scenario C. This price reduction was compensated by the cost for the lithium-ion storage, which increases the overall price in each scenario approximately by the factor of 10,6 in comparison to only using conventional grid reinforcement. The use of CHP instead of lithium-ion storage leads to a cost increase by the factor 5,7 compared to only using conventional grid reinforcement. It needs to be noted that the benefit of extant heat was not considered.
Comparing the EVCU distribution at the most sensitive node within the grid exposed only minor cost differences. The price difference between a distributed and concentrated placement varies by less than 7 %. Therefore, it is feasible to only consider the most sensitive nodes within a grid and use a concentrated load placement to approximate the cost for distributed load integration. A closer examination of the cost allocation for each grid reinforcement variant revealed, that the labor cost accounted for more than 50 % of the total cost for conventional grid reinforcement. When using lithium-ion storage or CHP, the respective technology accounted for more than 75 % of the total cost.

In this work, the integration of EVCQ and its resulting reinforcement cost were investigated for the cigre benchmark network. In the next step, the integration should be investigated for other benchmark grids, such as IEEE 342-node low voltage network test system [32]

or actual small power networks. These can be used to verify the cost results obtained through the nodes sensitivities. Furthermore, future research should investigate electric vehicle charging times and habits more precisely, in order to provide additional insight into load requirements.

It should also be considered, that the geographical location of the grid influences the price structure. For different reinforcement locations such as rural or denser urban areas (downtown), new conventional grid reinforcement prices should be compiled. Additionally, the cost benefit through the extant heat from CHP is also an important consideration.

References

Books

[1] Crastan, V.: *Elektrische Energieversorgung 1 : Netzelemente, Modellierung, stationäres Verhalten, Bemessung, Schalt- und Schutztechnik*, Springer Vieweg; Berlin, 2015.

[2] Doppelbauer, M.: *Grundlagen der Elektromobilität: Technik, Praxis, Energie und Umwelt*, Springer Vieweg; Berlin, 2020.

[3] Hofmann, L.: *Elektrische Energieversorgung / Lutz Hofmann ; Band 1: Grundlagen, Systemaufbau und Methoden, De Gruyter Studium*, De Gruyter Oldenbourg; Berlin, 2019.

[4] Hofmann, L.: *Elektrische Energieversorgung / Lutz Hofmann ; Band 2: Betriebsmittel und ihre quasistationäre Modellierung, De Gruyter Studium*, De Gruyter Oldenbourg; Berlin, 2019.

[5] Hofmann, L.: *Elektrische Energieversorgung / Lutz Hofmann ; Band 3: Systemverhalten und Berechnung von Drehstromsystemen, De Gruyter Studium*, De Gruyter Oldenbourg; Berlin, 2019.

[6] Kaufmann, W.: *Planung öffentlicher Elektrizitätsverteilungs-Systeme*, VWEW-Verlag; Frankfurt am Main, 1995.

[7] Kohn, W. and Öztürk, R.: *Grafische Darstellungen einer Verteilung*, Springer Berlin Heidelberg; Berlin, Heidelberg, 2016.

[8] Oeding, D. and Oswald, B. R.: *Elektrische Kraftwerke und Netze*, Springer Vieweg; Berlin, 2016.

[9] Oswald, B. R.: *Berechnung von Drehstromnetzen : Berechnung stationärer und nichtstationärer Vorgänge mit Symmetrischen Komponenten und Raumzeigern, Lehrbuch*, Springer Vieweg; Wiesbaden, 2017.

[10] Oswald, B. R.: *Netzberechnung : Berechnung stationärer und quasistationärer Betriebszustände in Elektroenergieversorgungsnetzen, mit 67 Bilder, 12 Tabellen und 5 Übungsaufgaben mit Lösung*, Zach GmbH & Co.; Berlin, 1992.

[11] Peterson, C. and Thomas, J. L.: *Aluminum Wire Tables*, National Bureau of Standards, Washington D.C., 1972.

[12] Sterner, M. and Stadler, I.: *Energiespeicher - Bedarf, Technologien, Integration*, Springer Vieweg; Berlin, 2017.

[13] Thomopoulos, N. T.: *Statistical Distributions : Applications and Parameter Estimates*, Springer; Cham, 2017.

[14] Wietschel, M. and Ullrich, S. J.: *Energietechnologien der Zukunft : Erzeugung, Speicherung, Effizienz und Netze, Lehrbuch*, Springer Vieweg; Wiesbaden, 2015.

University Publications

[15] Grahn, P.: *Electric Vehicle Charging Modeling*, 2014.

[16] Schlömer, G., Hofmann, L., and Witzmann, R.: *Planung von optimierten Niederspannungsnetzen*, 2017.

[17] Schnabel, S.: *Ein techno-ökonomisches Modell zur Netzplanung unter Berücksichtigung regulierter Netzentgelte - Ein integrierter Ansatz im Rahmen der wertorientierten Unternehmensführung am Beispiel der 110-kV-Verteilnetzebene*, 2013.

[18] Wolter, M.: *Agent based energy management systems, Berichte aus der Elektrotechnik*, Aachen, 2012.

[19] Wolter, M.: *Grid state identification of distribution grids, State identification of distribution grids, Berichte aus der Elektrotechnik*, Aachen, 2008.

Papers

[20] Adetokun, B. B., Ojo, J. O., and Muriithi, C. M.: *Reactive Power-Voltage-Based Voltage Instability Sensitivity Indices for Power Grid With Increasing Renewable Energy Penetration, IEEE Access*, *IEEE Access*, IEEE Access 8 (2020), pp. 85401–85410.

[21] Draz, M. and Albayrak, S.: *A Power Demand Estimator for Electric Vehicle Charging Infrastructure*, 2019 IEEE Milan PowerTech, IEEE; 2019, pp. 1–6.

[22] Dudek, E.: *The Flexibility of Domestic Electric Vehicle Charging: The Electric Nation Project, IEEE Power and Energy Magazine*, *IEEE Power and Energy Magazine*, IEEE Power and Energy Magazine 19.4 (2021), pp. 16–27.

[23] Fasthuber, D.: *Integration der Ladeinfrastruktur in das elektrische Energiesystem, Integration of the charging infrastructure into the electrical energy system, Elektrotech. Inftech., e & i Elektrotechnik und Informationstechnik*, *Elektrotech. Inftech., e & i Elektrotechnik und Informationstechnik*, Elektrotech. Inftech., e & i Elektrotechnik und Informationstechnik 137.4-5 (2020), pp. 156–160.

[24] Hardman, S.: *Investigating the decision to travel more in a partially automated electric vehicle, Transportation Research Part D: Transport and Environment*, *Transportation Research Part D: Transport and Environment*, Transportation Research Part D: Transport and Environment 96 (2021).

[25] Hardman, S. et al.: *A review of consumer preferences of and interactions with electric vehicle charging infrastructure* (2018).

[26] Hardman, S. et al.: *A review of consumer preferences of and interactions with electric vehicle charging infrastructure* (2018).

[27] Leveringhaus, T. and Hofmann, L.: *Comparison of methods for state prediction: Power Flow Decomposition (PFD), AC Power Transfer Distribution factors (AC-PTDFs), and Power Transfer Distribution factors (PTDFs)*, 2014 IEEE PES Asia-Pacific Power and Energy Engineering Conference (APPEEC), 2014, pp. 1–6.

[28] Nejabatkhah, F., Li, Y. W., and Wu, B.: *Control Strategies of Three-Phase Distributed Generation Inverters for Grid Unbalanced Voltage Compensation*, *IEEE Transactions on Power Electronics* 31.7 (2016), pp. 5228–5241.

[29] Nikitha, L. et al.: *Effect of electrical vehicle charging on power quality*, 2017 International Conference on Circuit ,Power and Computing Technologies (ICCPCT), 2017, pp. 1–6.

[30] Pau, M., Ponci, F., and Monti, A.: *Impact of Network Parameters Uncertainties on Distribution Grid Power Flow*, 2019 International Conference on Smart Energy Systems and Technologies *SEST*, IEEE; 2019, pp. 1–6.

[31] Salehi, J. and Haghifam, M.-R.: *Long term distribution network planning considering urbanity uncertainties, International Journal of Electrical Power and Energy Systems*, *International Journal of Electrical Power and Energy Systems*, International Journal of Electrical Power and Energy Systems 42.1 (2012), pp. 321–333.

[32] Schneider, K., Phanivong, P., and Lacroix, J.-S.: *IEEE 342-node low voltage networked test system*, 2014 IEEE PES General Meeting | Conference & Exposition, IEEE; 2014, pp. 1–5.

[33] Sok, V. and Tayjasanant, T.: *Determination of optimal siting and sizing of energy storage system in PV-connected distribution systems considering minimum energy losses*, 2017 14th International Conference on Electrical Engineering/Electronics, Computer, Telecommunications and Information Technology $ECTI - CON$, IEEE; 2017, pp. 451–454.

[34] Stock, D. S.: *Entwicklung eines flexiblen Optimierungswerkzeuges zur nichtlinearen mathematischen Mehrzieloptimierung in der Netzführung und Netzplanung* (2020).

[35] Tugend, S. et al.: *Spannungsregelung im Niederspannungsnetz auf Basis eines Spannungsbeobachters* (2015).

[36] Wang, Y. et al.: *Impact of Conductor Temperature Time–Space Variation on the Power System Operational State*, *Energies* 11.4 (2018).

[37] Wolter, M.: *Cost-effective grid state identification of mean voltage grids by using sensitivity analysis, Kostengünstige Identifikation des Zustands von Mittelspannungsnetzen mit dezentrales Einspeisung durch Sensitivitätsanalyse*, EuroPES, IASTED International Conference on European Power and Energy Systems, 7, ACTA Press; Anaheim, 2007, pp. 217–221.

Websites

[38] Blockheitskraftwerk24: BHKW Platzbedarf und Laustärke, 2021, [Online]
Avaiable at: https://blockheizkraftwerk24.com/bhkw-platzbedarf-lautstaerke/ [Accessed: 11.10.2021].

[39] Blockheizkraftwerk24: BHKW Wartung, 2021, [Online]
Avaiable at: https://blockheizkraftwerk24.com/bhkw-wartung/ [Accessed: 05.10.2021].

[40] BMWi: Was ist das NOVA-Prinzip?, 2021, [Online]
Avaiable at: https://www.bmwi.de/Redaktion/DE/FAQ/Netzausbau/faq-netzausbau-03.html [Accessed: 08.10.2021].

[41] Bundesministerium der Finanzen: AfA-Tabelle für die allgemein verwendbaren Anlagegüter, 2021, [Online]
Avaiable at: https://www.bundesfinanzministerium.de/Content/DE/Standardartikel/Themen/Steuern/Weitere_Steuerthemen/Betriebspruefung/AfA-Tabellen/Ergaenzende-AfA-Tabellen/AfA-Tabelle_AV.html [Accessed: 21.09.2021].

[42] Bureau of Labor Statistics US Department of Labor: International Comparision of Hourly Compensation Cost in Manufacturing, 2011, 2021, [Online]
Avaiable at: https://www.bls.gov/news.release/pdf/ichcc.pdf [Accessed: 07.10.2021].

[43] EnergieAgentur NRW GmbH: Hinweise zur Wirtschaftlichkeitsbetrachtung von Kraft-Wärme-Kopplungsanlagen mit fossilen Brennstoffen, 2021, [Online]
Avaiable at: https://www.energieagentur.nrw/content/anlagen/Wirtschaftlichkeit_KWK_Unternehmen.pdf [Accessed: 21.09.2021].

[44] Europian Commission: Communication from the Commission to the European Parliament, the council, the European and social committee and the committee of the regions, 2020, [Online]
Avaiable at: https://eur-lex.europa.eu/legal-content/EN/TXT/?uri=CELEX:52020DC0562 [Accessed: 07.09.2021].

[45] Georgia State University: Resistivity and Temperature Coefficient at 20°C, 2021, [Online]
Avaiable at: http://hyperphysics.phy-astr.gsu.edu/hbase/Tables/rstiv.html [Accessed: 10.09.2021].

[46] Hesselman: Starkstromkabel NAYY-J/O nach VDE 0276-603, 2021, [Online]
Avaiable at: https://www.hesselmann.de/data-download/produktinfo/he-nayy.pdf [Accessed: 07.09.2021].

[47] Orsted: Wasserstoff marsch, 2021, [Online]
Avaiable at: https://energiewinde.orsted.de/trends-technik/power-to-gas-audi-werlte [Accessed: 11.10.2021].

[48] UNFCCC: The Paris Agreement, 2016, [Online]
Avaiable at: https://unfccc.int/process-and-meetings/the-paris-agreement/the-paris-agreement [Accessed: 07.09.2021].

[49] Zaehlerschrank: Erdkabel NAYY (Aluminium), 2021, [Online]
Avaiable at: https://www.zaehlerschrank24.de/ [Accessed: 11.09.2021].

Others Resources

[50] *Regierungsprogramm Elektromobilität*, 2011, [Online]
Avaiable at: https://www.bmwi.de/Redaktion/DE/Downloads/P-R/regierungsprogramm-elektromobilitaet-mai-2011.pdf?__blob=publicationFile&v=6 [Accessed: 07.09.2021], BMWi;

[51] *Energiewirtschaftsgesetzes*, 2005, [Online]
Avaiable at: https://www.gesetze-im-internet.de/enwg_2005 [Accessed: 07.09.2021].

[52] *Gesetzentwurf der Bundesregierung Entwurf eines Gesetzes zum Aufbau einer gebäudeintegrierten Lade- und Leitungsinfrastruktur für die Elektromobilität*, 2020.

[53] *Benchmark Systems for Network Integration of Renewable and Distributed Energy Resources*, CIGRE; 2014.

[54] *Commission Regulation (EU) 2017/1485*, European Commission; 2017.

[55] *UIC Report - Electricity Infrastructure*, Agency for the Cooperation of Energy Regulators; 2015.

[56] *DIN 18015-1, Elektrische Anlagen in Wohngebäuden – Teil 1: Planungsgrundlagen*, Beuth Verlag GmbH; 2013-09.

[57] *Verkabelungsgrad des Stromnetzes in Deutschland nach Spannungsebene im Jahresvergleich 1993 und 2013*, Bundesverband der Energie- und Wasserwirtschaft e.V.; 2014.

[58] *Evaluierung der Kraft-Wärme-Kopplung: Analysen zur Entwicklung der Kraft-Wärme-Kopplung in einem Energiesystem mit hohem Anteil erneuerbarer Energien*, Fraunhofer Publica; 2019.

[59] *Vorlesung: Plannung und Führung von elektrischen Netzen, Leistungsflussberechnung Teil 1*, Institut für Elektrische Energiesysteme; 2020.

[60] *Internal Documents Dahmen Rohrleitungsbau GmbH & Co. KG*, 2021.

[61] *Anzahl der Elektroautos in Deutschland von 2011 bis 2021*, Kraftfahrt-Bundesamt; 2021.

[62] *Der Fahrzeugbestand im Überblick am 1. Januar 2021 gegenüber dem 1. Januar 2020*, Kraftfahrt-Bundesamt; 2021.

[63] *E-Home Energy Projekt 2020*, CIRED Workshop 2012; Lisbon, Portugal, 2017.

[64] *DIN VDE 0298-4, Strombelastbarkeit von Kabeln und Leitungen*, DIN-VDE-0298-4, Beuth Verlag GmbH; 2013.

[65] *DIN-EN-50169, Merkmale der Spannung in öffentlichen Elektrizitätsversorgungsnetzen*, DIN-EN-50160, Beuth Verlag GmbH; 2020.

[66] *DIN VDE 0100-722, Errichten von Niederspannungsanlagen*, VDE Verlag; 2013-09.

[67] *Understanding electricity markets in the EU*, European Parliament; 2016.

[68] *HV and LV Phase Imbalance Assessment*, 2015, [Online]
Avaiable at: https : / / www . spenergynetworks . co . uk / userfiles / file / HVandLVPhaseImbalanceAssessment16.pdf [Accessed: 19.09.2021], SP Energy Networks;

[69] *Die Umwelt in Europa - Zustand und Ausblick 2020*, Europäische Umweltagentur; 2020.

[70] *Treibhausgasemissionen sinken 2020 um 8,7 Prozent*, Umweltbundesamt; 2020.

[71] *Bevölkerung in Deutschland nach Anzahl der PKW im Haushalt von 2017 bis 2020*, VuMA; 2020.

8 Appendix

8.1 Grid Parameters

Table 8.1 Connections and line parameters of residential feeder of European LV distribution network benchmark [53]

Line segment	Node from	Node to	Conductor ID	length [m]	Installation
1	R1	R2	UG1	35	UG 3-ph
2	R2	R3	UG1	35	UG 3-ph
3	R3	R4	UG1	35	UG 3-ph
4	R4	R5	UG1	35	UG 3-ph
5	R5	R6	UG1	35	UG 3-ph
6	R6	R7	UG1	35	UG 3-ph
7	R7	R8	UG1	35	UG 3-ph
8	R8	R9	UG1	35	UG 3-ph
9	R9	R10	UG1	35	UG 3-ph
10	R3	R11	UG3	30	UG 3-ph
11	R4	R12	UG3	35	UG 3-ph
12	R12	R13	UG3	35	UG 3-ph
13	R13	R14	UG3	35	UG 3-ph
14	R14	R15	UG3	30	UG 3-ph
15	R6	R16	UG3	30	UG 3-ph
16	R9	R17	UG3	30	UG 3-ph
17	R10	R18	UG3	30	UG 3-ph

Table 8.2 Load parameters of European LV residential distribution network [53]

Conductor ID/ Installation		Phase impedance matrix after Kron reduction [Ω/km]		
		A	B	C
UG1 / 3-ph	A	0.616 + j0.588	0.131 + j0.306	0.141 + j0.245
	B	0.131 + j0.306	0.628 + j0.566	0.147 + j0.276
	C	0.141 + j0.245	0.147 + j0.276	0.650 + j0.527
UG3 / 3-ph	A	2.137 + j0.776	0.125 + j0.453	0.133 + j0.406
	B	0.125 + j0.453	2.146 + j0.771	0.138 + j0.447
	C	0.133 + j0.406	0.138 + j0.447	0.138 + j0.447

Table 8.3 Load parameters of European LV residential distribution network [53]

Node	Apparent Power, S [kVA]	Power Factor, φ
R1	200	0,95
R11	15	0,95
R15	52	0,95
R16	55	0,95
R17	35	0,95
R18	47	0,95

8.2 Characteristic Residential Consumer Loads

Table 8.4 Stress assumption and convergency factor by (WE = Housing-Units) [3]

Household variation	Max. power draw $P_{\mathrm{S,WE}}$	Max. power share $P_{\mathrm{maxLA,WE}}$	convergency factor g_∞
EG 1: weak electrification	5 kW	$0,7 \ldots 0,9 \frac{\mathrm{kW}}{\mathrm{WE}}$	$0,15 \ldots 0,20$
EG 2: medium electrification (lights and cooking)	5 kW	$1,0 \ldots 1,2 \frac{\mathrm{kW}}{\mathrm{WE}}$	$0,12 \ldots 0,15$
EG 3: full electrification (without heating)	30 kW	$1,8 \ldots 2,0 \frac{\mathrm{kW}}{\mathrm{WE}}$	$0,06 \ldots 0,07$
Full electrification	30 kW	$1,8 \ldots 2,0 \frac{\mathrm{kW}}{\mathrm{WE}}$	$0,06 \ldots 0,07$

8.3 Standards and Guidelines

Table 8.5 Conversion factor f for multiple ground laid cables [64]

Number of cabes	2	3	4	5	6	8	10
Conversion factor	0,86	0,76	0,71	0,67	0,64	0,6	0,57

8.4 Electrical Equipment Parameters

Table 8.6 Transformer parameters [16]

S_{rT} [kVA]	U_{rTHV} [kV]	U_{rTLV} [kV]	u_{k} [%]	P_{vK} [W]	P_{vL} [kV]	I_{idle} [A]
630	20	0,4	4,6	4740	635	1,1
1000	20	0,4	5,0	6780	960	1,8
1200	20	0,4	5,0	9500	1140	2,7
1600	20	0,4	6,0	14200	1500	3,5
2000	20	0,4	6,0	16900	2000	4,0
2500	20	0,4	6,0	19000	2200	4,0

Table 8.7 Low voltage cable parameters [46][53][16][49]

Designation/ID	A [mm^2]	$I_{\text{th}}[kA]$	R' [Ω/km]	L' [mH/km]	Price [€/m]
UG1	-	0,338	0,16	0,261	18,87
UG3	-	0,138	0,82	0,271	4,06
NAYY-J 4X25 SW	25	0,102	1,20	0,280	4,01
NAYY-J 4X35 SW	35	0,123	0,87	0,271	4,32
NAYY-J 4X50 SW	50	0,144	0,64	0,271	5,46
NAYY-J 4X70 SW	70	0,179	0,44	0,262	7,07
NAYY-J 4X95 SW	95	0,215	0,32	0,261	8,98
NAYY-J 4X120 SW	120	0,245	0,25	0,256	10,68
NAYY-J 4X150 SW	150	0,275	0,21	0,256	13,17
NAYY-J 4X185 SW	185	0,313	0,16	0,256	16,26
NAYY-J 4X240 SW	240	0,364	0,13	0,254	21,72
NAYY-J 4X300 SW	300	0,419	0,10	0,279	30,59

8.5 Electrical Equipment Cost

Table 8.8 Transformer cost for a lifespan of 60 years [16]

Transformer	Price [€]
630 kVA	18 750
1000 kVA	20 750
1200 kVA	21 750
1600 kVA	25 750
2000 kVA	27 750
2500 kVA	30 080
Building cost	15 000

Table 8.9 Construction cost for grid expansion [60]

Category	Prince [€/m]
Trench	79,04
Assembly pit	10,50
Pulling cable	10,50
Couplings	5,00
Back-filling	10,20
Diverse	30,00
Construction-site facilities	7 %
Total	152,50